Highlights

- δD_{wax} of topsoil *n*-acids was characterised 13 northern boreal sites
- Vegetation *n*-acid abundances and distributions were characterised
- Mosses dominate *n*-acids contributions to northern boreal soils
- Mean $\varepsilon_{wax/MAP}$ is -93±10‰, -101±11‰ and -95±11‰ for *n*-$C_{24,26,28}$ acids, respectively
- Smaller $\varepsilon_{wax/MAP}$ values are observed at higher latitudes

Net fractionation of hydrogen isotopes in *n*-alkanoic acids from soils in the northern boreal forest

Aleesha Bakkelund[a], Trevor J. Porter[a*], Duane G. Froese[b], Sarah J. Feakins[c]

[a]Department of Geography, University of Toronto Mississauga, Mississauga, ON, L5L 1C6, Canada

[b]Earth and Atmospheric Sciences, University of Alberta, Edmonton, AB, T6G 2E3, Canada

[c]Department of Earth Sciences, University of Southern California, Los Angeles, CA, 90089, USA

*Corresponding author. Tel.: +1-905-828-5314 (T.J. Porter);

Email address: trevor.porter@utoronto.ca

Abstract

Plant-derived *n*-alkyl lipids are well-preserved in sedimentary archives, and their stable hydrogen isotope ratio (δD_{wax}) is a proxy for precipitation δD and climate. Net fractionation of H isotopes between plant source water and *n*-alkyl lipids ($\varepsilon_{wax/water}$) is the largest uncertainty for interpreting this proxy and depends on plant type and environment. Although popular proxies, *n*-alkanoic acids (*n*-acids) are less frequently calibrated in modern environments than *n*-alkanes. We constrain the net fractionation ($\varepsilon_{wax/MAP\ –\ Mean\ Annual\ Precipitation}$) for the northern boreal forest based on *n*-$C_{24,26,28}$ acids in topsoils from a 13-site network in Yukon, Alaska and Northwest Territories (60-68°N). *n*-Acid homologue distributions for common boreal plants (gymnosperm trees, shrubs, forbs, C3 grasses and mosses) show that soil *n*-acids are dominated by mosses, but with a reduced carbon preference index compared to fresh mosses, possibly owing to post-depositional degradation. Regionally averaged $\varepsilon_{wax/MAP}$ values are –93±10‰, –101±11‰ and –95±11‰ for *n*-$C_{24,26,28}$ acids, respectively, which are similar to values reported from low and high latitude regions. We find that $\varepsilon_{wax/MAP}$ for *n*-$C_{26,28}$ acids (but not *n*-C_{24}) is significantly ($p \leq 0.05$) smaller with increasing latitude and decreasing mean annual temperature, factors that covary across our network. Since latitude is typically known for ancient deposits, we parsed the dataset to obtain latitude-specific $\varepsilon_{wax/MAP}$ values for 60-64°N (–107±8‰ for *n*-C_{26}; and –101±8‰ for *n*-C_{28}) and 65-68°N (–94±11‰ for *n*-C_{26}; and –89±10‰ for *n*-C_{28}). These soil-derived values are relevant for hydroclimate reconstructions using fossil *n*-acids in paleosols from a comparable paleoflora and latitude.

Keywords: northern boreal forest; plant waxes; *n*-alkanoic acids; stable hydrogen isotopes; compound-specific isotope analysis; net fractionation

1. Introduction

Stable isotope ratios of hydrogen (D/H) and oxygen ($^{18}O/^{16}O$) in precipitation are well-established tracers for hydroclimatic variables, including precipitation amount and air temperature (Dansgaard, 1964; Craig and Gordon, 1965). Hydrogen isotopes derived from meteoric waters are preserved in the long straight-chain hydrocarbons (*n*-alkanoic acids, *n*-alkanes, and *n*-alcohols) that make up the cuticular waxes of plants (Hou et al., 2008; Sachse et al., 2012; Wilkie et al., 2013), which has made fossil plant waxes a popular proxy in paleo-hydroclimate studies. Fossil plant waxes are well-preserved in sedimentary archives (e.g., relict permafrost, paleosols, lacustrine sediment cores, etc.) over geologic timescales (e.g. Yang and Huang, 2003; Tierney et al., 2008; Vonk et al., 2017) owing to their hydrophobicity, inertness, and resistance to biodegradation (Huang et al., 1997; Nguyen Tu et al., 2017). Long-chain (>20 carbon atoms) *n*-alkanoic acids (hereafter *n*-acids) with a characteristic predominance of even-number C-chains, and *n*-alkanes with a predominance of odd-number C-chains, are both derived from a common precursor (Zhou et al., 2010). Together these compounds form major constituents of the waxy coating within and on top of the cuticle of plant leaves

and, thus, both are used as biomarkers for terrestrial plants (Eglinton and Hamilton, 1963). *n*-Alkyl hydrogens do not exchange readily under 150°C (Sessions et al., 2004) allowing isotopic signals of synthesis to be retained in sedimentary storage.

The hydrogen isotopic composition of plant waxes (δD_{wax}) is offset from the hydrogen isotopic composition of precipitation (δD_{precip}) by a large negative fractionation. This offset is referred to as the net (or apparent) fractionation ($\varepsilon_{wax/precip}$) and varies regionally with climate and vegetation type (Sachse et al., 2012). Terrestrial plants absorb water from soil moisture, which is ultimately derived from precipitation. Evaporation can enrich deuterium (D) in soil water, however many plants do not use evaporatively-enriched soil water (Feakins and Sessions, 2010), although it may be a factor in some shallow rooted plants such as grasses (Smith and Freeman, 2006). Hydrogen isotopes are generally not fractionated during uptake of source water by roots (White et al., 1985; Ehleringer and Dawson, 1992; Roden et al., 2000a); however, transpiration results in D-enrichment of leaf waters (Feakins and Sessions, 2010) and the magnitude of this enrichment depends on relative humidity, isotopic composition of the ambient water vapour, and leaf geometry (Barbour et al., 2004; Kahmen et al., 2008; Sachse et al., 2012). *n*-Acid precursors inherit H isotopes from leaf water, but a series of biosynthetic fractionations then results

79 in D-depletion of the resulting *n*-alkyl lipids relative to leaf water (Chikaraishi
80 et al., 2004a; Zhou et al., 2010; Sachse et al., 2012).

81 Large variability in $\varepsilon_{wax/precip}$ has been noted between different groups of
82 plants and photosynthetic pathways. On average, *n*-C_{29} alkanes produced by
83 shrubs are more enriched in deuterium compared to trees, forbs and
84 graminoids (Sachse et al., 2012) given the same source water. Therefore,
85 changes in vegetation type and abundance within a catchment can result in
86 variability in sedimentary δD_{wax} that is unrelated to δD_{precip} (Fornace et al.,
87 2014). For δD_{wax}-based paleoclimate reconstructions, this underscores the need
88 to use $\varepsilon_{wax/precip}$ values that are appropriate to the plant community and
89 climate, to enable robust estimates of δD_{precip} (Feakins, 2013; Nichols et al.,
90 2014). The $\varepsilon_{wax/precip}$ parameter has been calibrated extensively for low and mid
91 latitude ecosystems, but there are only a few high-latitude examples, limiting
92 our ability to interpret high-latitude δD_{wax} records.

93 Previous calibration studies have constrained $\varepsilon_{wax/precip}$ in various ways.
94 Growth-chamber experiments have tested select species, under known
95 conditions where irrigation water and other factors (e.g., light, humidity) are
96 controlled, and the δD_{wax} of new foliage is measured and used to determine
97 $\varepsilon_{wax/water}$ (e.g., Yang et al., 2009). Natural ecosystem surveys have compared the
98 δD_{wax} of leaves and δD of plant water (e.g., xylem water) to calculate $\varepsilon_{wax/xylem}$
99 (e.g., Feakins and Sessions, 2010; Daniels et al., 2017). Other sedimentary

100 approaches have compared the δD_{wax} of integrated waxes in surface (*ca.*
101 modern) sediments with a best estimate of local δD_{precip} in order to estimate
102 $\varepsilon_{wax/precip}$ for the plant community as represented in sediments (e.g., Shanahan
103 et al., 2013; Wilkie et al., 2013). All are valid approaches with different
104 strengths and limitations. For example, $\varepsilon_{wax/water}$ can be directly determined for
105 specific plants in growth-chamber experiments and ecosystem surveys, but
106 fossil waxes in the geologic record are subject to other uncertainties related to
107 post-depositional processes and wax inputs from other vegetation. Conversely,
108 $\varepsilon_{wax/precip}$ estimates from sedimentary waxes (e.g., soil, lake sediment) integrate
109 all wax inputs and pre-depositional processes, but source water δD cannot be
110 directly measured and, thus, must be estimated to constrain $\varepsilon_{wax/precip.}$ The δD
111 value of amount-weighted Mean Annual Precipitation (δD_{MAP}) is commonly
112 used as an approximation for source water δD (e.g., meta-analysis by Sachse et
113 al., 2012). For future reference, the term '$\varepsilon_{wax/MAP}$' is used when referring to net
114 fractionation estimates expressed relative to δD_{MAP} (measured or modelled).

115 In a survey of lake sediment cores in dwarf shrub-tundra catchments on
116 Baffin Island (62-74°N), Canadian High Arctic, Shanahan et al. (2013) found a
117 mean $\varepsilon_{wax/MAP}$ of –61‰, based on the mean δD_{wax} of *n*-C_{26} and -C_{28} acids. This
118 value is smaller than what is typical for herbaceous plants in low and middle
119 latitudes (Sachse et al., 2012). Shanahan et al. (2013) linked this observation to
120 an evapotranspiration effect on leaf water that was first observed in growth

121 chamber experiments by Yang et al. (2009) who found *n*-alkanes from
122 deciduous conifers under 24-hour light (simulating High Arctic conditions)
123 were up to 40‰ enriched compared to foliage grown in diurnal light conditions.

124 At a comparable latitude in northeastern Siberia (67.5°N), Wilkie et al.
125 (2013) found a $\varepsilon_{wax/MAP}$ of –95‰ for *n*-C_{30} acids for *ca.* modern lake sediments of
126 Lake El'gygytgyn, surrounded by tundra plants including lichen and
127 herbaceous taxa. From lacustrine core top sediments of tundra lakes in
128 northern Alaska (68.5°N), Daniels et al. (2017) observed larger $\varepsilon_{wax/MAP}$ values
129 of –118‰ for *n*-$C_{25\text{-}33}$ alkanes, and –114‰ for *n*-$C_{22\text{-}30}$ acids. Sachse et al. (2004)
130 report the largest $\varepsilon_{wax/MAP}$ values from lacustrine sediments from taiga and
131 tundra catchments in Fennoscandia (61-69°N) with a mean of –125‰ for *n*-C_{29}
132 alkanes.

133 With the exception of the study on Baffin Island (Shanahan et al., 2013), net
134 fractionation estimates from most high-latitude sites (>60°N) are comparable
135 in value to observations from mid to low latitude sites with values ranging
136 from –90 to –130‰ for both *n*-alkanes (Chikaraishi et al., 2004b; Pagani et al.,
137 2006; Sachse et al., 2006; Smith and Freeman, 2006; Hou et al., 2007; Kahmen
138 et al., 2013; Gao et al., 2014; Feakins et al., 2016b; Freimuth et al., 2017) and
139 *n*-acids (Hou et al., 2007; Feakins et al., 2014, 2016b; Gao et al., 2014;
140 Freimuth et al., 2017). Additionally, studies spanning large latitudinal
141 gradients do not appear to support a strong relationship between latitude and

net fractionation (Sachse et al., 2006; Liu et al., 2016), which suggests that light-dependent controls on net fractionation may be unique to certain high-latitude environments. More work is needed to understand this diversity in high-latitude environments.

One high-latitude ecosystem that remains largely unstudied in the *n*-alkyl literature is the northern boreal forest. The boreal forest covers an estimated 1.2 billion hectares of the Earth, spanning large portions of North America and Eurasia (Soja et al., 2007). Furthermore, the boreal ecosystem was present in the Western sub-Arctic during the Holocene and past interglacials (Schweger et al., 2011; Kaufman et al., 2012), and at higher latitudes during the Pliocene (Csank et al., 2011, 2013), which makes it an important target for modern calibration studies to exploit fossil boreal δD_{wax} as a paleoenvironmental proxy.

We address this knowledge gap with a study of *n*-acids from modern vegetation and top-soils from southern Yukon to the northernmost extent of boreal treeline in Northwest Territories. We focus specifically on *n*-acids because Pinaceae gymnosperm trees (e.g., *Picea*, *Pinus* and *Larix*), which dominate the boreal canopy, are known to produce negligible amounts of *n*-alkanes (Diefendorf et al., 2011) and, thus, are likely to be unrepresented in soil *n*-alkanes (Schäfer et al., 2016). Soil surveys have been widely used for calibration of δD_{wax} elsewhere (Chikaraishi and Naraoka, 2006; Jia et al., 2008; Peterse et al., 2009; Rao et al., 2009; Bai et al., 2011; Ponton et al., 2014;

Schwab et al., 2015) to understand the plant wax signals incorporated into soils. Our research objectives are two-fold: (1) to characterize the *n*-acid chain length distributions of common boreal vegetation types in order to understand the major contributor(s) to sedimentary lipid pools; and (2) to quantify the net fractionation of *n*-acids in northern boreal soils. This work will inform future paleoclimate studies based on fossil *n*-acids sourced from boreal paleoflora.

2. Methods

2.1 Study area

Soil and vegetation samples were collected from thirteen locations in the Yukon, Northwest Territories, and Alaska (Fig. 1), spanning 60.3 to 68.3°N. The climate of the study region is cold and semi-arid, characterized by short, cool summers and long, cold winters (Fig. 2). Mean annual temperature (MAT) ranges from –8.4 in the north to –1.7°C in the south, with average daily temperatures above freezing from May to September based on ERA-Interim data (Fig. 1; Table 1; Dee et al., 2011). Average growing season temperatures range from 4 to 12°C. Daylight hours at the summer solstice range from 19 hours in southern Yukon to 24 hours in the north (Wahl, 2004). The northern half of the site network (>65°N) falls within the continuous permafrost zone, and the more southern sites are in the discontinuous or sporadic permafrost zones (Brown et al., 1997).

As our study region encompasses a large range of latitudes and mean temperatures, the start and end points of the growing season (timing and duration of leaf wax synthesis) also vary regionally. The growing season is primarily limited by minimum temperatures above the freezing mark. In the southern end of our transect (e.g., Whitehorse) minimum daily temperatures are above freezing from May 18 to September 24 (duration = 129 days), and in the northern end (e.g., Inuvik) from May 27 to September 23 (duration = 119

190 days) (Dee et al., 2011). However, other abiotic factors such as sunlight and
191 ground temperatures (influencing unfrozen water availability) also influence
192 the timing of biosynthesis during the growing season.

193 The Alaska Range and St. Elias Mountains represent a significant barrier to
194 the advection of Pacific moisture into continental Yukon. Areas of low elevation
195 receive 250-300 mm of precipitation annually, while higher elevations receive
196 more, up to 400-500 mm, based on WorldClim 2 data (Fick and Hijmans, 2017).
197 Over 75% of precipitation falls between May and September (Wahl, 2004). Peak
198 summer (JJA) average relative humidity differs by 13% (62 to 74%) between
199 sites based on CliMond data (Table 1, Fig. 1; Kriticos et al., 2012).

200 The study sites are mature subarctic woodlands, which are broadly
201 representative of the northern boreal forest ecology and span a range of
202 latitudes and climate conditions which allows us to examine the range of
203 variability in net fractionation within this ecotype. The sites are primarily
204 spruce (*Picea glauca* and *Picea mariana*) and moss dominated woodlands
205 characterized by moderately open canopies. *Pinus contorta* and *Larix laricina*
206 trees are dominant or co-dominant at two of our sites. The sub-canopy typically
207 includes a thick (5-15 cm) moss ground cover with patches of Poaceae grass and
208 Ericaceae forbs, and sparse shrub cover including alder (*Alnus* sp.), willow
209 (*Salix* sp.) and dwarf birch (*Betula nana*). The mosses associated with subarctic
210 woodlands are diverse and include *Sphagnum* hummock varieties (e.g.,

211 *Sphagnum fuscum and S. balticum*) and feathermoss varieties (e.g.,
212 *Pleurozium schreberi, Ptilium crista-castrensis, Tomentypnum nitens,* and
213 *Dicranum polysetum*) with the assemblage being influenced by soil moisture
214 and woodland successional stage (Black and Bliss, 1978; Turetsky et al., 2012).
215 Most sites are relatively flat with moist but unsaturated, organic-rich soils, and
216 underlain by clastic parent material (clay, silts).

217 *2.2 Sampling methods*

218 Soil samples were collected from most sites in July 2014, and from the LC
219 and SH sites in July 2016 and SP site in July 2017. Soil samples were collected
220 to examine the homologue distribution and hydrogen isotope ratios of long
221 chain (C_{24}, C_{26}, and C_{28}) *n*-acids. Soils were collected from ~30 cm soil pits in 3-
222 10 cm intervals, depending on the thickness of the O-horizon; the O- and A-
223 horizons were collected separately. Soil pits were dug in open areas within 2 m
224 of the canopy dominant tree, and in close proximity to shrubs and forbs and
225 these soil pit criteria were held constant across our site network. A single pit
226 was sampled at most sites, in order to compare the O and A horizons at a
227 representative location. We do not describe within-site heterogeneity such as
228 may vary with plant cover, plant growth-limiting factors, or microtopography.
229 Instead, we prioritized a large number of sites across a long transect to
230 characterise latitudinal variability in net fractionation across the northern
231 boreal forest.

232 Vegetation samples were collected at the same sites to examine the
233 distribution of *n*-acid homologues and to determine which plant types are
234 contributing most to soils. Fresh leaves or needles with minimal evidence of
235 damage or decomposition were collected from up to three individual dominant
236 or co-dominant shrubs, trees, mosses, grasses and forbs within a ~5 m radius of
237 the soil pit. The isotopic composition of vegetation samples was not measured.
238 All vegetation and soil samples were collected using nitrile gloves and stored in
239 Whirlpak™ bags, chilled over ice in a field cooler, and shipped frozen to the
240 laboratory for processing and analysis.

241 *2.3 Vegetation sample classification*

242 Vegetation samples were classified as tree, shrub, moss, grass or forb. An
243 inventory of plant taxa sampled at each site is provided in the supplement
244 (Table S1). All trees were gymnosperms. White spruce (*Picea glauca*, $n = 33$;
245 here, 'n' refers to the number of individual *P. glauca* trees that were sampled
246 across the regional network) was dominant at all sites except TSI, MYO,
247 DHP174 and SP. Larch (*Larix Laricina,* $n = 1$) trees are dominant at the TSI
248 site. Black spruce (*Picea mariana*, $n = 3$) was co-dominant with white spruce at
249 MYO and DHP174. Lodgepole pine (*Pinus contorta*, $n = 1$) was co-dominant
250 with white spruce at SP. Shrub cover was sparse and variable, and included
251 willow (*Salix sp.,* $n = 20$), alder (*Alnus sp.*, $n = 5$) or dwarf birch (*Betula nana*, n
252 = 7). Mosses common in northern boreal woodlands are diverse, and an

253 inventory of all moss taxa at each site was not attempted. Fresh mosses (n =
254 12) were sampled from the top of the O horizon of our soil pits, and was mostly
255 identified as the red-stemmed feathermoss *Pleurozium schreberi*
256 (Hylocomiaceae); minor co-mingled fractions of *Tomentypnum nitens, Ptilium*
257 *crista-castrensis* and *Dicranum polysetum* were also observed. Grasses in this
258 region are Poaceae and use the C3 metabolic pathway (n = 13). All forbs were
259 Ericaceae, including crowberry (*Empetrum nigrum*, n = 1), lingonberry
260 (*Vaccinium vitis-idaea*, n = 2), blueberry (*Vaccinium uliginosum*, n = 1), and
261 Labrador tea (*Rhododendron sp.*, n = 3).

262 *2.4 Lipid extraction*

263 Soil samples were freeze dried in a Labconco freezone 2.5 unit. n-Acid
264 concentrations varied between soil samples. Initially, 5 g of dry, homogenized
265 sediment was subsampled for lipid extraction. Following the initial
266 quantification of n-acids by GC-FID (described below), additional sediment (up
267 to 60 g) was sometimes required to yield sufficient n-acid amounts for the
268 compound-specific isotope analysis.

269 Soil bound-lipids were extracted with 9:1 (v/v) Dicholoromethane
270 (DCM):Methanol (MeOH) by microwave-assisted heating (Milestone Ethos Up
271 unit) at 70°C for 20 minutes, and continuous magnetic stirring, a method
272 selected for optimal recovery (Chávez-Lara et al., 2018). Samples were then
273 centrifuged at 1800 RPM for 10 minutes to settle the sediment, and the

supernatant was removed and retained. The sediment sample was rinsed three to five additional times with DCM-MeOH, centrifuged and transferred to the collection vial. Excess solvent was evaporated under a gentle stream of N_2 gas.

Foliage samples were dried in paper bags in an oven at 60°C for 48 hours. Chopped, dry foliage (1 g) was submerged in DCM:MeOH (9:1, v/v) and agitated by Pasteur pipette pumping and the extract removed (repeated three times) to remove the epicuticular and intracuticular waxes (similar to the methods of Feakins and Sessions, 2010; Feakins et al., 2016a).

The total lipid extract was separated by column chromatography in a 5.75" borosilicate glass Pasteur pipette packed with Phenomenex 60 Å NH2 sepra stationary phase. The neutral fraction was eluted with 2:1 DCM:isopropanol, followed by the acid fraction with 4% formic acid in diethyl ether. The acid fraction was methylated to Fatty Acid Methyl Esters (FAMEs) using 5% hydrochloric acid and 95% methanol (δD_{MeOH} = –246.6‰, following methodology in Lee et al., 2017) at 60°C for 12 hours. The mixture was cooled and ~1 mL MilliQ water was added. Then, 1 mL hexanes was added and shaken vigorously for 30 s, to partition the FAMEs into the hexanes and this liquid-liquid extraction was repeated (three times) to ensure recovery. The extract was passed through a column of anhydrous sodium sulfate to remove any water. The extract was purified by column chromatography with 5% water-deactivated 100-200 mesh silica gel, and the FAMEs were eluted with 3 column

rinses of hexanes and then DCM. The saturated FAMEs were further purified by column chromatography with silver nitrate on silica gel (+230 mesh), also eluted with hexanes and DCM.

2.5 Quantification and isotope analysis

FAMEs were analysed at the University of Toronto Mississauga with a Gas Chromatograph (Thermo Trace 1310) Flame Ionization Detector (GC-FID), equipped with a Programmable Temperature Vaporizing (PTV) injector and a Rxi-5 ms column (30 m x 0.25 mm, film thickness 1 µm). The FID results were normalised to known quantities of an in-house FAME standard (n-C_{17}, -C_{21}, -C_{25} and -C_{29} FAMEs). For all samples, we calculated the average chain length (ACL = $\Sigma(C_n \times n)/\Sigma C_n$, where C_n is the abundance for chain-lengths from n = 20-34), modal chain length (C_{max}), and the carbon preference index (CPI = ([$C_{20, 22, 24, 26, 28, 30}$] + [$C_{22, 24, 26, 28, 30, 32}$])/(2 × [$C_{21, 23, 25, 27, 29, 31}$])), the latter a measure of degradation (Bray and Evans, 1961).

Compound-specific hydrogen isotope ratios were measured at the University of Southern California using a Thermo Scientific Trace GC equipped with a PTV inlet operated in solvent split mode and a Rxi-5 ms column (30 m x 0.25 mm x 0.25 µm), connected via a GC Isolink with pyrolysis (1400°C), via a Conflo IV to an Isotope Ratio Mass Spectrometer (Delta V IRMS). The H_3^+ factor was measured daily to check for linearity and remained close to 8 ppm mV^{-1}. H_2 reference peaks were injected at the beginning and end of each sample

316 run on the GC-IRMS, with two used for standardization between sample and
317 standard runs. Hydrogen isotope ratios are reported in delta notation: $\delta D = (R_{sample} - R_{standard})/R_{standard}$, where R is the ratio of deuterium to protium
319 ($^2H/^1H$). Precision of replicate sample injections was typically better than 1‰.
320 Data were normalized to the VSMOW-SLAP hydrogen isotopic scale using the
321 A3 mix alkane standard with δD values ranging from –233.7 to –46.3‰
322 (supplied by A. Schimmelmann, Indiana University, Bloomington). The RMS
323 error of replicate analyses of the A3 mix was typically better than 4‰ over the
324 month of analysis. Hydrogen atoms added by methylation were corrected for by
325 mass balance: $\delta D_{wax} = \delta D_{meas}\,(2i + 2\text{-}3 \times \delta D_{MeOH})/(2i\text{-}1)$, where δD_{meas} is the
326 normalized δD value of the FAME and i is the number of carbon atoms in the
327 fatty acid molecule of interest.

328 *2.6 Net fractionation*

329 Net (or apparent) fractionation was calculated for each soil sample based on
330 the general formula: $\varepsilon_{wax/MAP} = (\delta D_{wax} + 1)/(\delta D_{MAP} + 1) - 1$, where δD_{wax} is a
331 measured value from *n*-acids recovered from the soils and δD_{MAP} (amount-
332 weighted mean annual precipitation δD) is a best estimate of average source
333 waters available to plants for each of our sites. Compared to unweighted mean
334 annual precipitation, δD_{MAP} is biased to warm-season values, reflecting higher
335 precipitation totals in summer (Fig. 2), but also accounts for significant inputs
336 of D-depleted snowmelt to the ground in springtime (Mackay, 1983). Further

rationale for the δD_{MAP} assumption is discussed in Section 4.2. We used the Online Isotopes in Precipitation Calculator (OIPC; Bowen, 2018; Bowen and Wilkinson, 2002; Bowen and Revenaugh, 2003) to estimate monthly δD_{precip} (Fig. 2) and δD_{MAP} for our sites, which is common practice in other δD_{wax} calibration studies (e.g. Sachse et al., 2004; Shanahan et al., 2013; Freimuth et al., 2017). The OIPC provides interpolated δD_{precip} estimates constrained by empirical data from GNIP (Global Network for Isotopes in Precipitation) stations, including local stations at Whitehorse, Mayo, and Inuvik (Fig. 1). δD_{MAP} ranges from –160 ± 2‰ at Lost Chicken, to –176‰ at Inuvik, with a regional, all-site average of –168‰ ($1\sigma = 6$) (Table 2). This region is characterized by a large seasonal range in monthly δD_{precip} of 113‰. Minimum δD_{precip} occurs in January and ranges from –203 to –252‰ between sites, and maximum δD_{precip} occurs in either June or September and ranges from –123 to –132‰ between sites (Fig. 2).

3. Results

3.1 Vegetation

Vegetation samples yielded long chain *n*-C_{20} to -C_{34} acids with notable differences in chain length distribution between vegetation types (Fig. 3). All vegetation types demonstrate the expected predominance of even-over-odd C-chain *n*-acid homologues with mean CPI values ranging from 10.5 to 14.2. Mosses and shrubs have the shortest modal chain lengths (C_{max} = 24 and 26 for mosses and shrubs, respectively); grasses (C_{max} = 28) and forbs and trees have a longer dominant chain length (C_{max} = 30). Mosses and shrubs have the lowest ACL of 24.8 and forbs had the highest ACL of 29.3 (Fig. 3, Table S2). Shrubs yielded the greatest average concentration of total long-chain *n*-acids ($\sum_{C20\text{-}C34}$) per gram of dry foliage (716 µg g^{-1}), followed by forbs (398.1 µg g^{-1}), grasses (156.6 µg g^{-1}), trees (132.2 µg g^{-1}), and mosses (60.2 µg g^{-1}) (Tables S1 for inventory of sampled plants, and Table S2 for *n*-acid data averaged by vegetation type and site). Site-averaged ACL and CPI for most plant types are not significantly correlated with site-specific climatic (temperature, relative humidity, precipitation amount) or geographic (latitude, longitude, elevation) variables, except the ACL of shrubs which is significantly correlated ($p \leq 0.05$) with latitude, longitude, elevation, mean annual temperature and annual RH (see Table S3 for all correlations).

3.2 Modern soils

n-Acids with carbon chain-lengths between C_{20} and C_{30} are the most abundant in the average soil sample (averaged across all sites, equal weight given to all sites) with a modal chain length of 24, and an ACL of 24.2 ± 0.5 (Fig. 3; see Table S4 for site averages, and Table S5 for all samples). Most of this distribution is centered between C_{22} and C_{26}, and relative abundances are especially low (3% or less) for chain-lengths greater than C_{30}. The all-site average CPI is 2.8 ± 0.9 indicating even over odd chain length predominance, but is notably smaller than the CPI values observed for fresh vegetation which were greater than 10. The same homologue distribution is also observed for all-site averages calculated separately for the O and A soil horizons (Table S6). Site-averaged ACL and CPI values calculated for the O and A horizons separately are not significantly different ($p < 0.05$; 2-sample t-tests). As was true for most vegetation samples, site-averaged soil ACL and CPI values are not significantly correlated with any of the climatic or geographic variables (see Table S3).

In terms of absolute abundance, total long-chain *n*-acid ($\sum_{C20\text{-}C34}$) concentrations were highly variable between sites, ranging from 17.2 to 267.4 μg g^{-1} (Table S4). Likewise, absolute concentrations for individual *n*-acids also varied between sites, for example, ranging from 6-94 μg g^{-1} for n-C_{24}, 3-25 μg g^{-1} for n-C_{26}, and 2-21 μg g^{-1} for n-C_{28}.

Site-averaged *n*-acid δD_{wax} values ranged from –256 to –234‰ (mean = –246‰, 1σ = 7‰) for *n*-C_{24}, –264 to –241‰ (mean = –253‰, 1σ = 7‰) for *n*-C_{26}, and –260 to –238‰ (mean = –248‰, 1σ = 6‰) for *n*-C_{28} acids (see Table S4 for site-averages, and Table S5 for individual soil samples from each site). Site-averaged *n*-C_{24}, C_{26} and C_{28} acid δD_{wax} values are not significantly different ($p \leq 0.05$; 2-sample t-test) between the O- and A- horizon (Table S6). Site-averaged δD_{wax} values are not significantly correlated with the climate or geographic variables, except *n*-C_{26} δD_{wax} which correlates with mean annual precipitation (Table S3).

3.3 Net fractionation

Net fractionation values ($\varepsilon_{wax/MAP}$) were calculated for soil-derived *n*-C_{24}, -C_{26} and -C_{28} acids for each soil sample (O and A horizons), which were then used to calculate site averages. Site averages were used to calculate regional averages (each site contributing equally to the regional average).

Site-averaged (including O and A horizon soils) $\varepsilon_{wax/MAP}$ values range from –110 to –71‰ for *n*-C_{24}, –122 to –80‰ for *n*-C_{26}, and –111 to –77‰ for *n*-C_{28} acids (Table 2). The regional 'all-site' average $\varepsilon_{wax/MAP}$ values are –93‰ (1σ = 10), –101‰ (1σ = 11) and –95‰ (1σ = 11) for *n*-C_{24}, C_{26} and C_{28} acids, respectively (Table 2). We find no significant differences between regional $\varepsilon_{wax/MAP}$ averages for the three major *n*-acids (t-tests, $p \leq 0.05$). Further, we find no significant differences (t-tests, $p \leq 0.05$) between regional $\varepsilon_{wax/MAP}$ values when calculated

for O and A horizons separately (see regional O and A horizon $\varepsilon_{wax/MAP}$ values in Table S6).

We find spatial trends in $\varepsilon_{wax/MAP}$ across the network of sites. Site-averaged $\varepsilon_{wax/MAP}$ is significantly ($p \leq 0.05$) correlated with latitude for *n*-C_{26} and -C_{28} ($r = 0.62$ and 0.56, respectively; Fig. 4a), with MAT for *n*-C_{26} and -C_{28} ($r = -0.55$ and -0.59, respectively; Fig. 4d), and with elevation but for *n*-C_{26} only ($r = -0.61$) (Fig. 4b). The $\varepsilon_{wax/MAP}$ values are not significantly correlated with precipitation amount, relative humidity, or mean growing season temperature (Fig. 4c, 4e, and 4f). $\varepsilon_{wax/MAP}$ values are generally smaller at higher latitudes, lower mean elevations and lower MATs – factors that tend to covary across our network of sites.

4. Discussion

4.1 n-Acid abundance in vegetation and soils

Although *n*-alkyl homologue distributions aren't taxonomically diagnostic (Eglinton and Hamilton, 1963), some generalisations can be made between plant groups. For example, grasses, herbs and forbs produce a high proportion of high molecular weight (>C_{30}) *n*-alkanes and -acids compared to other plants (Eglinton and Hamilton, 1963; Diefendorf et al., 2011; Bush and McInerney, 2013), while mosses produce abundant lower molecular weight *n*-alkanes (C_{23} and C_{25}) and *n*-acids (C_{22} and C_{24}) (Pancost et al., 2002; Bush and McInerney, 2013; Vonk et al., 2017). These tendencies are also reflected in our modern vegetation and soil samples (Fig. 3).

A comparison of *n*-acid relative abundances from our type-averaged vegetation and average soil (0-30 cm below surface, including A and O layers) shows that the distribution of *n*-acids in soils (Fig. 3f) closely resembles that of mosses (Fig. 3d), with a C_{24} modal chain-length, followed by C_{22} and then C_{26} in relative abundance. This distribution is unique to mosses (Pancost et al., 2002). We find this pattern even when the O and A horizons are examined separately (see Table S6) and, persists when we average the data from the two horizons, suggesting that mosses dominate soils throughout the profile.

Shrubs have a modal chain-length of C_{26} and high proportions of C_{24} and C_{28}, (Fig. 3b) which is inconsistent with the homologue pattern in soils. We do

460 find a spatial variation in the distribution of *n*-acid homologues, but only in
461 shrubs, which have a significantly longer ACL at higher latitudes ($r = 0.8$, $p < 0.01$) or colder MAT ($r = -0.77$, $p < 0.01$) (see Table S3 for all correlations).
463 Other studies have noted significant correlations between plant ACL and
464 hydroclimate gradients (e.g., Bush and McInerney, 2015; Feakins et al., 2016b),
465 which is thought to reflect a functional role long *n*-alkyl chains have in
466 mitigating leaf-water loss. However, the fact that soil ACL across our network
467 of sites is poorly correlated (n.s.) with the climate and geographic variables
468 (contrary to shrubs) is further evidence that shrubs are not a major *n*-acid
469 contributor to boreal soils at the average site.

470 Grasses produce mainly *n*-C_{26} and -C_{28} acids (Fig. 3a), which is inconsistent
471 with the soil *n*-acid pattern, and suggests grasses are not a major *n*-acid source.
472 This is not surprising, as grasses prefer dry, raised tussocks which represent a
473 negligible area of the boreal forest floor.

474 Overall, we note that *n*-acids with chain-lengths >C_{30} are negligible in
475 boreal soils, with no detectable *n*-C_{34} acids at all sites, no detectable *n*-C_{32} acids
476 at five sites, and no detectable *n*-C_{30} acids at three sites (Table S2). These
477 higher molecular weight *n*-acids feature prominently in forbs and trees (Figs.
478 3c and 3e) but are largely absent in boreal soils (Fig. 3f). Thus, it is unlikely
479 forbs or trees are major *n*-acid contributors to soils.

480 The evidence points strongly to mosses as a primary *n*-acid contributor to
481 boreal soils. Although mosses have the lowest average *n*-acid ($\sum_{C20\text{-}C34}$)
482 concentration per dry mass (60.2 μg g^{-1}), they are spatially ubiquitous and
483 dominate the O horizon in terms of raw biomass, which likely overcompensates
484 for its lower absolute *n*-acid concentrations compared to other plants. The low
485 stature and physical connection of mosses at the surface of the O-layer may
486 also favour greater transfer (and representation) of *n*-acids in boreal soils.

487 Substantial inter- and intra-site variability is noted in soil *n*-acid ($\Sigma_{C20\text{-}C34}$)
488 concentrations and chain length distributions, consistent with the
489 heterogeneous nature of soils observed elsewhere (Lehmann et al., 2008;
490 Schäfer et al., 2016), which we attempt to correct for by averaging soils from
491 various depths from the O and A soil horizons (1 to 9 soil samples per site).
492 Site-averaged soil *n*-acid concentrations vary from 17.2 to 267.4.0 μg g^{-1}
493 between sites (Table S4), which likely reflects differences in rates of lipid
494 production, deposition, and mineralization and degradation, including the
495 effects of bacterial activity for example. The $\Sigma_{C20\text{-}C34}$ concentrations are on
496 average slightly higher for the O horizon compared to the A horizon – 133.0 ±
497 105 μg g^{-1} versus 74.8 ± 81 μg g^{-1}, respectively – which may indicate a higher
498 ratio of *n*-acid accumulation to degradation in the O horizon; however, this
499 difference is not statistically significant ($p = 0.31$). The overall range of soil
500 $\Sigma_{C20\text{-}C34}$ n-acid concentrations by site (17.2 to 267.4 μg g^{-1}) is in line with total

soil *n*-acid concentrations from the litter and Ah soil horizons of grasslands, and conifer and deciduous forests in Western Europe which can range from ~10-200 μg g^{-1} (Schäfer et al., 2016).

Previous studies have demonstrated that microbial activity result in substantial decreases in *n*-acid concentrations between vegetation and soil (Chikaraishi and Naraoka, 2006; Schäfer et al., 2016; Nguyen Tu et al., 2017). Preferential degradation of long chain *n*-acids (>C_{28}) has been suggested by previous studies (Chikaraishi and Naraoka, 2006; Nguyen Tu et al., 2017). The site-averaged CPI of soils in this study (2.8 ± 0.9) is significantly lower (t-test, $p < 0.05$) than the average CPI observed in fresh mosses (10.5 ± 3.3), which has the lowest CPI of all major vegetation types (Fig. 3). This suggests that some microbial degradation or other pedogenic factors may be affecting *n*-acid chain length distributions, with a disproportionate loss of the relatively abundant even chain lengths, resulting in a reduced CPI. The same effect was observed for soil *n*-acids along a transect from northern Croatia to southern Sweden (Schäfer et al., 2016). However, the processes by which this degradation occurs in soils has not been fully explored in the literature.

4.2 Source water δD and timing of lipid synthesis

Before discussing the $\varepsilon_{wax/MAP}$ results, we briefly discuss the relevance of δD_{MAP} as a source water approximation for sub-Arctic plants. The relevance of this assumption depends largely on: (i) the phenology (timing and duration) of

leaf wax synthesis of the plants that contribute *n*-alkyls to soils; and (ii) mean soil water δD at the time of leaf wax synthesis; both of which are not well known in this region.

Most plant wax phenology studies have focused on *n*-alkanes from mid-latitude environments. *n*-Alkane synthesis in angiosperm trees (Tipple et al., 2013; Freimuth et al., 2017) and C3 grasses (Gamarra and Kahmen, 2017) is associated with leaf development, which for many plants is concentrated towards the start of the growing season; however, in temperate regions with long growing seasons (e.g., 9 months), leaf wax concentrations and homologue patterns can continue to evolve for the first half of the growing season (Sachse et al., 2015). To our knowledge, only one study has assessed *n*-acid phenology and found that *n*-acids are synthesized continuously throughout the growing season in temperate angiosperms (Freimuth et al., 2017). If *n*-acids are also produced continuously in northern boreal woodland plant types throughout the growing season, this would mean the δD source water assumption should also align with mean growing season soil waters (i.e., mid-May to late-September, Methods 2.1).

Average soil water δD in sub-Arctic regions is also not well known, but is thought to reflect changing seasonal inputs of spring snowmelt and summer rainwater, mixing with remnant pore waters from the previous year (frozen *in situ* during the freezeback), and evaporative enrichment of near-surface soil

543 waters in the mid-summer. In temperate alpine forests in Switzerland, which
544 experience freeze-thaw, Brinkmann et al. (2018) demonstrated that comparable
545 meteoric water contributions from summer (50%) and prior fall and winter
546 months (40%) are represented in soil and xylem waters of *Fagus sylvatica* and
547 *Picea abies* trees during the growing season. In a shrub-tundra environment in
548 N. Alaska, Daniels et al. (2017) demonstrated that *Eriophorum vaginatum* (C3
549 grass) and *Betula nana* (shrub) xylem waters in the mid-growing season (mid-
550 July) were comparable to δD_{MAP}, while August xylem waters were enriched
551 relative to δD_{MAP} by ~+10‰; data were not collected for the first half of the growing
552 season (June 3-July 17) when soil and xylem waters were likely depleted compared to
553 δD_{MAP}. Both case studies offer some empirical support for the notion that mean
554 soil and xylem waters integrate a blend of year-round precipitation in alpine
555 and low-Arctic regions, and that δD_{MAP} offers a reasonable approximation for
556 δD source water in cold-regions. We assume this approximation also applies to
557 northern boreal woodlands, but acknowledge that future ecohydrology studies
558 are needed to better substantiate this assumption.

559 *4.3 Net fractionation*

560 Our regional average $\varepsilon_{wax/MAP}$ values calculated for n-$C_{24,26,28}$ acids (–93 ±
561 10‰, –101 ± 11‰, and –95 ± 11‰, respectively) are all within error the mean
562 $\varepsilon_{wax/MAP}$ of –96 ± 8‰ (based on *n*-C_{30} acids) reported by Wilkie et al. (2013) from
563 lake sediments in N.E. Siberia, and within two standard errors of the $\varepsilon_{wax/MAP}$

564 of –114 ± 13‰ (based on *n*-$C_{22\text{-}30}$ acids) reported by Daniels et al. (2017) from
565 lake sediments in N. Alaska (Fig. 5). All of these $\varepsilon_{wax/MAP}$ values are far more
566 negative than the mean $\varepsilon_{wax/MAP}$ of –61 ± 20‰ (based on *n*-C_{26} and -C_{28} acids)
567 reported by Shanahan et al. (2013) from lake sediments on Baffin Island (Fig.
568 5). *n*-$C_{25\text{-}31}$ alkanes in surface sediments of northern (> 60°N) Fennoscandian
569 lakes reported by Sachse et al. (2006) are characterised by an average $\varepsilon_{wax/MAP}$
570 value of –125 ± 7‰ (Fig. 5), which is significantly larger than the *n*-acid-based
571 $\varepsilon_{wax/MAP}$ values from Wilkie et al. (2013) and in this study. Some studies have
572 found *n*-acids are significantly more enriched in D by ~25 ± 16‰ compared to
573 *n*-alkanes from the same leaves (Chikaraishi and Naraoka, 2007), which could
574 explain the smaller $\varepsilon_{wax/MAP}$ values in *n*-acids vs. *n*-alkanes (Fig. 5). However,
575 the average $\varepsilon_{wax/MAP}$ calculated from lake sediment *n*-alkanes (–118 ± 9‰) in N.
576 Alaska is only slightly larger than the mean $\varepsilon_{wax/MAP}$ value based on *n*-acids (–
577 114 ± 13‰) (Daniels et al., 2017). Therefore, factors other than compound class
578 may be responsible for the larger *n*-alkane $\varepsilon_{wax/MAP}$ values in Fennoscandia.

579 At broader scales, our regional $\varepsilon_{wax/MAP}$ values are also similar to n-acid (*n*-
580 C_{28} or longer) net fractionations reported from tropical and temperate sites
581 which range from –90 to –121‰ (mean: –105‰) (Hou et al., 2008; Feakins et
582 al., 2014, 2016a; Gao et al., 2014). Collectively, this argues for a similar net
583 fractionation in *n*-acids across broad geographic scales and ecosystem types.
584 However, our $\varepsilon_{wax/MAP}$ results show some evidence of geographic and/or climatic

585 dependencies, indicating that spatial factors may influence net fractionation at
586 regional scales.

587 On average, δD_{MAP} is more negative at higher latitudes or lower MATs (Figs.
588 6a and c), which is typical at mid- to high-latitudes (Dansgaard, 1964), and
589 specifically in this region (Porter et al., 2016), reflecting preferential rainout of
590 heavy isotopologues as moist air travels away from the ocean source towards
591 cooler, higher latitudes. Conversely, δD_{wax} for *n*-C_{26} and -C_{28} acids is slightly
592 more positive at higher latitudes or colder MATs (Figs. 6b and 6d), although
593 these δD_{wax} trends are not statistically significant ($p \geq 0.05$). The combination
594 of the opposing trends in δD_{MAP} and δD_{wax} results in smaller $\varepsilon_{wax/MAP}$ values at
595 higher latitudes or lower MATs. However, due to collinearity between latitude
596 and MAT ($r = -0.91$, $p \leq 0.01$) it is not clear which is the driving variable. A
597 significant correlation is also observed between $\varepsilon_{wax/MAP}$ and elevation for *n*-C_{26}
598 acids only ($r = -0.63$, $p < 0.05$). However, this correlation is also confounded by
599 collinearities with latitude ($r = -0.82$, $p \leq 0.01$) and MAT (0.65, $p \leq 0.05$). There
600 are no known physical linkages between $\varepsilon_{wax/MAP}$ and elevation (or dependent
601 variables not already included in our correlation analysis; Table S3) and, thus,
602 perhaps the most likely explanation for this correlation is random co-variability
603 in combination with latitude and MAT collinearities. We focus the remainder of
604 our discussion on possible linkages between latitude or MAT on $\varepsilon_{wax/MAP}$, which
605 have been evaluated to some extent in previous studies.

606 Latitude does not have a direct influence on $\varepsilon_{wax/MAP}$. However, other
607 variables that co-vary with latitude such as sunlight availability may have an
608 effect (Sessions, 2006; Yang et al., 2009). Across our network of sites, June-
609 August total sunlight hours ranges from 1608 hours (average 17.5 hours/day)
610 at the most southern site to 1973 hours (average 21.5 hours/day) at the most
611 northern site (USNO-AA, 2018). There are two mechanisms discussed in the
612 literature linking sunlight and $\varepsilon_{wax/MAP}$. Growth-chamber experiments (Yang et
613 al., 2009) have found smaller net fractionations in plants exposed to increased
614 light levels (simulating a high-latitude environment), an effect that is thought
615 to be due to enhanced transpiration and D-enrichment of leaf waters, resulting
616 in higher δD_{wax} and smaller $\varepsilon_{wax/MAP}$ values. This mechanism was invoked by
617 Shanahan et al. (2013) to explain unusually small $\varepsilon_{wax/MAP}$ values (average = –
618 61 ± 20‰) calculated for *n*-$C_{26\text{-}28}$ acids from lake sediments on Baffin Island (62-
619 73°N). However, evidence for strong leaf water evaporative enrichment effects
620 on $\varepsilon_{wax/water}$ in natural ecosystem surveys is generally lacking (Feakins and
621 Sessions, 2010).

622 A second mechanism linking sunlight to $\varepsilon_{wax/MAP}$ relates to usage of stored
623 carbohydrates. Under restricted light, plants use more stored carbohydrates
624 (which are associated with an overall smaller biochemical fractionation, ε_{bio}) as
625 feedstock for synthesizing plant waxes, leading to a smaller $\varepsilon_{wax/water}$ (Sessions,
626 2006; Cormier et al., 2018). However, this mechanism is inconsistent with the

627 sign of the latitude (sunlight)-$\varepsilon_{wax/MAP}$ response observed across our network of
628 sites, which shows smaller $\varepsilon_{wax/MAP}$ values at high latitudes where light is more
629 abundant.

630 The correlation between MAT and $\varepsilon_{wax/MAP}$ could reflect a direct effect of
631 temperature on ε_{bio}. However, previous studies of tree-ring cellulose δD have
632 specifically investigated this possibility and concluded that no such relation
633 exists (Roden et al., 2000b).

634 Although the physical drivers of $\varepsilon_{wax/MAP}$ variability across our network of
635 sites are not known, the reality of this variability implies that a single $\varepsilon_{wax/MAP}$
636 may not necessarily be appropriate for all boreal sites. This has implications
637 for interpreting fossil *n*-acid δD_{wax} records, since the use of a single $\varepsilon_{wax/MAP}$
638 value to reconstruct paleo-δD_{precip} from fossil δD_{wax} could introduce additional
639 uncertainties. Rather, a latitude-specific $\varepsilon_{wax/MAP}$ (for *n*-C_{26} and -C_{28} acids only)
640 may improve the accuracy of δD_{precip} reconstructions in northern boreal regions.
641 If we parse the *n*-C_{26} and -C_{28} datasets by latitude, a variable that is generally
642 well known for most geological applications (rather than temperature which
643 would need to be independently reconstructed), we find that sites < 65°N have
644 a significantly larger mean $\varepsilon_{wax/MAP}$ values than sites > 65°N (Fig. 4g). For the
645 southern sites (< 65°N, n = 7), we calculate mean $\varepsilon_{wax/MAP}$ values of –107 ± 8‰
646 for *n*-C_{26}, and –101 ± 8‰ for -C_{28} acids. For the northern sites (> 65°N, n = 6),

647 we calculate mean $\varepsilon_{wax/MAP}$ values of –94 ± 11‰ for *n*-C_{26}, and –89 ± 10‰ for -C_{28}
648 acids.

649

650 *4.4 Additional uncertainties in net fractionation*

651 While regional trends in $\varepsilon_{wax/MAP}$ are partially explained by latitude (r =
652 0.62 or ~38% of variance for *n*-C_{26} acids), a significant fraction of inter-site
653 variability in $\varepsilon_{wax/MAP}$ must be related to other factors, as discussed below.

654 Inter-site differences in minor wax contributions from the different
655 boreal vegetation types may contribute to soil $\varepsilon_{wax/MAP}$ variability. For example,
656 globally, *n*-alkane $\varepsilon_{C29/MAP}$ values for C3 grasses, forbs, trees and shrubs are –
657 149‰, –128‰, –121‰ and –99‰, respectively, or a 50‰ range between the C3
658 grasses and shrub end-members (Sachse et al., 2012). These differences in
659 $\varepsilon_{wax/MAP}$ owe to plant-specific differences in biochemical fractionation and the
660 fraction of enriched leaf water that imprints on *n*-alkyl precursors (Gamarra et
661 al., 2012), as well as rooting depth which can lead to major differences between
662 shallow versus deep-rooted plants in environments where near surface source
663 waters are evaporatively D-enriched (Nichols et al., 2010). For a shrub-tundra
664 environment in N. Alaska, Daniels et al. (2017) report a 64‰ range in $\varepsilon_{wax/xylem}$
665 values between C3 grasses (*Eriophorum vaginatum*; $\varepsilon_{C28/xylem}$ = –160‰) and
666 shrubs (*Betula nana*; $\varepsilon_{C28/xylem}$ = –96‰). These Alaskan *n*-acid $\varepsilon_{wax/xylem}$ values
667 are similar to global *n*-alkane $\varepsilon_{C29/MAP}$ values for C3 grasses and shrubs (Sachse

et al., 2012); therefore, a similarly large range in $\varepsilon_{wax/MAP}$ may be expected for grasses and shrubs in the boreal forest. It is possible some inter-site $\varepsilon_{wax/MAP}$ variance in our network owes to variable wax contributions from the minor plant types (e.g., C3 grasses and shrubs). However, C3 grasses occupy a small fraction of the boreal forest understorey, restricted to micro-topographic high points that are well drained, and likely do not contribute much biomass to soils. Conversely, shrubs occupy a larger area of the boreal understory and have the highest *n*-acid concentrations in fresh foliage of all vegetation types. Therefore, it seems more probable that shrubs would have a greater influence on the soil *n*-acid pool then other minor vegetation types such as C3 grasses.

Site slope, aspect and soil character (texture, compaction, permafrost) may also contribute to soil $\varepsilon_{wax/MAP}$ variability, since these variables have some implications for drainage (Christensen et al., 2013) and, therefore, soil water δD. During the spring melt, winter precipitation runs off sloped, impermeable sites more rapidly, whereas sites in flat areas or depressions with permeable soils are likely to retain more winter precipitation in soil water. In turn, soil *n*-acids from poorly drained sites may be expected to have larger $\varepsilon_{wax/MAP}$ due to a greater uptake of winter precipitation compared to well-drained sites. Future insights on soil-derived $\varepsilon_{wax/MAP}$ values may benefit from investigations of site specific and microtopographic effects on source water δD.

688 Inaccurate δD_{MAP} estimates may also contribute to inter-site variability
689 in $\varepsilon_{wax/MAP}$. We used δD_{MAP} estimates from the OIPC (Bowen and Revenaugh,
690 2003), an interpolated product that depends on available data from the local
691 GNIP stations. There are three GNIP stations in proximity to our network of
692 sites, including Inuvik, Mayo, and Whitehorse (Fig. 1). However, the number of
693 monthly records, continuity and temporal coverage of these records is highly
694 variable. For example, the Inuvik GNIP record holds 14 monthly observations
695 spanning the years 1986-1989, most (n = 8) of which are from 1988. Conversely,
696 Whitehorse has the best coverage with 95 monthly records with relatively
697 continuous coverage from 1961-1965 and 1985-1989. The spatial and temporal
698 inequities in the GNIP network leaves open the possibility that there may be
699 some regional bias in the δD_{MAP} isoscape, with implications for $\varepsilon_{wax/MAP}$.

700 Within-site $\varepsilon_{wax/MAP}$ variability is also substantial (1σ ranges from 2-15 ‰
701 depending on the homologue and site). Increasing the number of samples per
702 site would allow for a more robust mean $\varepsilon_{wax/MAP}$ estimate from each site, and
703 may reduce inter-site variability. However, considering the range of latitude
704 and climatic conditions covered by this transect, as well as the documented
705 heterogeneity of soils at even nanometer scales (Lehmann et al., 2008), the
706 inter- and intra- site variability we observe is not unexpected.

707 *4.5 Potential for paleoenvironmental applications*

The contiguous region of continental Yukon and Alaska that was unglaciated during the last full glacial, collectively known as Eastern Beringia, hosts an abundance of fossil-rich sediments spanning the last ca. 2.9 Ma (Elias, 2000; Matheus et al., 2003; Matthews et al., 2003; Zazula et al., 2003; Péwé et al., 2009; Schweger et al., 2011), which offers great potential for fossil wax-based paleoclimate reconstructions. By comparison, most other sub-Arctic regions lack Pleistocene surficial deposits due to the legacy of glacial scouring. The pre-50 ka chronology of deposits in Eastern Beringia is also exceptional, owing to datable ash beds from proximal volcanic sources (Froese et al., 2009; Preece et al., 2011). Recent studies in central Yukon have documented well-preserved *n*-alkanes and -acids from steppe-tundra paleoenvironments in relict permafrost deposits dating to Late Pleistocene cold stages (Pautler et al., 2014; Porter et al., 2016). However, this proxy has not been applied to Pleistocene interglacial paleosols in this region, which are reported at numerous locales (Schweger et al., 2011). Fossil pollen and macrofossil evidence reveals that *Picea* dominated woodlands, consistent with the majority of our sites, were typical during most interglacials in this region (Schweger et al., 2011). The $\varepsilon_{wax/MAP}$ constrained in our study represents an important first step toward interpreting interglacial paleosols in Eastern Beringia.

To date, most quantitative paleoclimate estimates from this region are based on the Modern Analogue Technique using fossil pollen (Viau et al., 2008)

729 or the Mutual Climate Range approach using fossil insects (Elias, 2000; Zazula
730 et al., 2011). However, pollen and midge reconstructions, like all paleoclimate
731 proxies, have uncertainties and do not always produce coherent paleoclimate
732 estimates in this region (see discussion by Porter et al., 2016). Fossil *n*-acids
733 provide an independent proxy that can be readily applied, in concert with more
734 traditional proxies (e.g., pollen and insect assemblages), to better resolve the
735 Quaternary history of this region.

5. Conclusions

This study analyzed *n*-acids from modern vegetation and soils from a network of 13 sites in Yukon, Alaska and Northwest Territories. The goals of this study were to better understand: (1) which plant types are the primary contributors of *n*-acids to northern boreal soils, and (2) the net fractionation of hydrogen isotopes in boreal soil *n*-acids. Regional soil surveys represent a powerful approach to constraining net fractionation as they integrate a large number of uncertainties that may influence sedimentary δD_{wax} variability, for example, due to differences in the relative contributions of major and minor plant types, post-depositional degradation, microtopography and drainage, and a wide range of climatic and geographic variables. The net fractionation values presented here are most directly applicable for δD_{MAP} reconstructions based on *n*-acids from boreal paleosols, as wax transport, sources and degradation may vary between soils and other depositional systems (e.g. lake sediments; Nguyen Tu et al., 2017).

The overall *n*-acid homologue pattern observed in boreal soils (O and A horizons) in this study is closely associated with the pattern observed in fresh mosses, which suggests mosses are a primary *n*-acid contributor to the average boreal soil. The overall net fractionation of soil δD_{wax} relative to δD_{MAP} ($\varepsilon_{wax/MAP}$) is –93 ± 10‰ for *n*-C_{24}, –101 ± 11‰ for -C_{26}, and –96 ± 11 ‰ for -C_{28} acids, respectively. We also observe spatial trends in $\varepsilon_{wax/MAP}$ for *n*-C_{26} and -C_{28} acids

(but not -C_{24}) with smaller $\varepsilon_{wax/MAP}$ values at higher latitudes or at lower mean annual temperatures, factors that co-vary across our network. Since latitude is generally well known over recent geologic timescales, this is a more pragmatic way to parse the dataset. We define two latitude-specific $\varepsilon_{wax/MAP}$ values, one for sites < 65°N and one for sites > 65°N. For the more southern group (60-64°N), $\varepsilon_{wax/MAP}$ is –107 ± 8 ‰ for *n*-C_{26} and –101 ± 8 ‰ for -C_{28} acids, respectively. For the northern group (65-68°N), $\varepsilon_{wax/MAP}$ is –94 ± 11 ‰ for *n*-C_{26} and –89 ± 10 ‰ for -C_{28} acids, respectively. These results will help inform δD_{wax} interpretations from fossil boreal *n*-acids, especially from paleosol deposits that are associated with the northern boreal woodland ecology.

Acknowledgements

Funding for this research includes a US National Science Foundation Grant NSF-EAR-1703141 to SF, Natural Science and Engineering Research Council (NSERC) Discovery grants to TP and DF, and a NSERC Canadian Graduate Scholarship to AB. We are grateful for field and lab assistance by Gerard Otiniano, Sasiri Bandara, Sean Walisser, Hyejung Lee, Sydney Clackett, and Kira Holland. We thank Merritt Turetsky for moss identification assistance. We also thank Associate Editor Philip Meyers and two anonymous reviewers for their constructive comments.

References

Bai, Y., Fang, X., Gleixner, G., Mügler, I., 2011. Effect of precipitation regime on δD values of soil n-alkanes from elevation gradients - Implications for the study of paleo-elevation. Organic Geochemistry 42, 838–845.

Barbour, M.M., Roden, J.S., Farquhar, G.D., Ehleringer, J.R., 2004. Expressing leaf water and cellulose oxygen isotope ratios as enrichment above source water reveals evidence of a Péclet effect. Oecologia 138, 426–435.

Bowen, G.J., 2018. The Online Isotopes in Precipitation Calculator, version 3.1. http://www.waterisotopes.org.

Bowen, G.J., Revenaugh, J., 2003. Interpolating the isotopic composition of modern meteoric precipitation. Water Resources Research 39, 1–13.

Bowen, G.J., Wilkinson, B., 2002. Spatial distribution of $\delta^{18}O$ in meteoric precipitation. Geology 30, 315–318.

Bray, E.., Evans, E.., 1961. Distribution of n-paraffins as a clue to recognition of source beds. Geochimica et Cosmochimica Acta 22, 2–15.

Brinkmann, N., Seeger, S., Weiler, M., Buchmann, N., Eugster, W., Kahmen, A., 2018. Employing stable isotopes to determine the residence times of soil water and the temporal origin of water taken up by *Fagus sylvatica* and *Picea abies* in a temperate forest. New Phytologist, doi:10.1111/nph.15255.

Brown, J., Ferrians, O.J., Heginbottom, J.A., Melnikov, E.S. (Eds.), 1997.

797 Circum-Pacific Map Series CP-45. U.S. Geological Survey in Cooperation
798 with the Circum-Pacific Council for Energy and Mineral Resources,
799 Washington, DC. Scale 1:10,000,000, sheet 1.

800 Black, R.A., Bliss, L.C., 1978. Recovery sequence of *Picea mariana* - *Vaccinium*
801 *uliginosum* forests after burning near Inuvik, Northwest Territories,
802 Canada. Canadian Journal of Botany 56: 2020-2030.

803 Bush, R.T., McInerney, F.A., 2013. Leaf wax *n*-alkane distributions in and
804 across modern plants: Implications for paleoecology and chemotaxonomy.
805 Geochimica et Cosmochimica Acta 117, 161-179.

806 Bush, R.T., McInerney, F.A., 2015. Influence of temperature and C4 abundance
807 on *n*-alkane chain length distributions across the central USA, Organic
808 Geochemistry 79, 65–73.

809 Chávez-Lara, CM, Holtvoeth, J, Roy, PD, Pancost, RD, 2018. A 27cal ka
810 biomarker-based record of ecosystem changes from lacustrine sediments of
811 the Chihuahua Desert of Mexico. Quaternary Science Reviews 191: 132-
812 143.

813 Chikaraishi, Y., Naraoka, H., 2006. Carbon and hydrogen isotope variation of
814 plant biomarkers in a plant-soil system. Chemical Geology 231, 190–202.

815 Chikaraishi, Y., Naraoka, H., 2007. $\delta^{13}C$ and δD relationships among three n-
816 alkyl compound classes (*n*-alkanoic acid, *n*-alkane and *n*-alkanol) of
817 terrestrial higher plants. Organic Geochemistry 38: 198–215.

818 Chikaraishi, Y., Naraoka, H., Poulson, S.R., 2004a. Hydrogen and carbon
819 isotopic fractionations of lipid biosynthesis among terrestrial (C3, C4 and
820 CAM) and aquatic plants. Phytochemistry 65, 1369–1381.

821 Chikaraishi, Y., Suzuki, Y., Naraoka, H., 2004b. Hydrogen isotopic
822 fractionations during desaturation and elongation associated with
823 polyunsaturated fatty acid biosynthesis in marine macroalgae.
824 Phytochemistry 65, 2293–2300.

825 Christensen, A.F., He, H., Dyck, M.F., Lenore Turner, E., Chanasyk, D.S.,
826 Naeth, M.A., Nichol, C., 2013. In situ measurement of snowmelt
827 infiltration under various topsoil cap thicknesses on a reclaimed site.
828 Canadian Journal of Soil Science 93, 497–510.

829 Cormier, M.-A., Werner, R.A., Sauer, P.E., Gröcke, D.R., M.C., L., Wieloch, T.,
830 Schleucher, J., Kahmen, A., 2018. ^{2}H fractiontions during the biosynthesis
831 of carbohydrates and lipids imprint a metabolic signal on the $\delta^{2}H$ values of
832 plant organic compounds. New Phytologist. doi:10.1111/nph.15016

833 Craig, H., Gordon, L.I., 1965. Deuterium and oxygen 18 variations in the ocean
834 and the marine atmosphere, Stable Isotopes in Oceanographic Studies and
835 Paleotemperatures. Spoleto, Italy.

836 Csank, A.Z., Patterson, W.P., Eglington, B.M., Rybczynski, N., Basinger, J.F.,
837 2011. Climate variability in the Early Pliocene Arctic: Annually resolved
838 evidence from stable isotope values of sub-fossil wood, Ellesmere Island,

839 Canada. Palaeogeography, Palaeoclimatology, Palaeoecology 308, 339-349.

840 Csank, A.Z., Fortier, D., Leavitt, S.W., 2013. Annually resolved temperature
841 reconstructions from a late Pliocene-early Pleistocene polar forest on Bylot
842 Island, Canada. Palaeogeography, Palaeoclimatology, Palaeoecology 369,
843 313–322.

844 Daniels, W.C., Russell, J.M., Giblin, A.E., Welker, J.M., Klein, S., Huang, Y.,
845 2017. Hydrogen isotope fractionation in leaf waxes in the Alaskan Arctic
846 tundra. Geochimica et Cosmochimica Acta 213, 216–236.

847 Dansgaard, W., 1964. Stable isotopes in precipitation. Tellus 16, 436–468.

848 Dee, D.P., Uppala, S.M., Simmons, A.J., Berrisford, P., Poli, P., Kobayashi, S.,
849 Andrae, U., Balmaseda, M.A., Balsamo, G., Bauer, P., Bechtold, P.,
850 Beljaars, A.C.M., van de Berg, L., Bidlot, J., Bormann, N., Delsol, C.,
851 Dragani, R., Fuentes, M., Geer, A.J., Haimberger, L., Healy, S.B.,
852 Hersbach, H., Hólm, E. V., Isaksen, L., Kållberg, P., Köhler, M.,
853 Matricardi, M., Mcnally, A.P., Monge-Sanz, B.M., Morcrette, J.J., Park,
854 B.K., Peubey, C., de Rosnay, P., Tavolato, C., Thépaut, J.N., Vitart, F.,
855 2011. The ERA-Interim reanalysis: Configuration and performance of the
856 data assimilation system. Quarterly Journal of the Royal Meteorological
857 Society 137, 553–597.

858 Diefendorf, A.F., Freeman, K.H., Wing, S.L., Graham, H.V., 2011. Production of
859 *n*-alkyl lipids in living plants and implications for the geologic past.

860 Geochimica et Cosmochimica Acta 75, 7472-7485.

861 Eglinton, G., Hamilton, R.J., 1963. The distribution of alkanes. In: Swain, T.
862 (Ed.), Chemical Plant Taxonomy. Academic Press, pp. 187-217.

863 Ehleringer, J.R., Dawson, T.E., 1992. Water uptake by plants: perspectives
864 from stable isotope composition. Plant, Cell & Environment 15, 1073–1082.

865 Elias, S.A., 2000. Late Pleistocene climates of Beringia, based on analysis of
866 fossil beetles. Quaternary Research 53, 229–235.

867 Feakins, S.J., Sessions, A.L., 2010. Controls on the D/H ratios of plant leaf
868 waxes in an arid ecosystem. Geochimica et Cosmochimica Acta 74, 2128-
869 2141.

870 Feakins, S.J., 2013. Pollen-corrected leaf wax D/H reconstructions of northeast
871 African hydrological changes during the late Miocene. Palaeogeography,
872 Palaeoclimatology, Palaeoecology 374, 62–71.

873 Feakins, S.J., Kirby, M.E., Cheetham, M.I., Ibarra, Y., Zimmerman, S.R.H.,
874 2014. Fluctuation in leaf wax D/H ratio from a southern California lake
875 records significant variability in isotopes in precipitation during the late
876 Holocene. Organic Geochemistry 66, 48–59.

877 Feakins, S.J., Patrick, L., Salinas, N., Shenkin, A., Blonder, B., Goldsmith,
878 G.R., Ponton, C., Arvin, L.J., Sin, M., Peters, T., West, A.J., Martin, R.E.,
879 Enquist, B.J., Asner, G.P., Malhi, Y., 2016a. Plant leaf wax biomarkers

880 capture gradients in hydrogen isotopes of precipitation from the Andes and
881 Amazon. Geochimica et Cosmochimica Acta 182, 155–172.
882 Feakins, S.J., Peters, T., Sin, M., Shenkin, A., Salinas, N., Girardin, C.A.J.,
883 Patrick, L., Blonder, B., Enquist, B.J., Martin, R.E., Asner, G.P., Malhi, Y.,
884 2016b. Production of leaf wax n-alkanes across a tropical forest elevation
885 transect. Organic Geochemistry 100, 89–100.
886 Fick, S.E., Hijmans, R.J., 2017. WorldClim 2: new 1-km spatial resolution
887 climate surfaces for global land areas. International Journal of
888 Climatology 37, 4302–4315.
889 Fornace, K.L., Hughen, K.A., Shanahan, T.M., Fritz, S.C., Baker, P.A., Sylva,
890 S.P., 2014. A 60,000-year record of hydrologic variability in the Central
891 Andes from the hydrogen isotopic composition of leaf waxes in Lake
892 Titicaca sediments. Earth and Planetary Science Letters 408, 263–271.
893 Freimuth, E.J., Diefendorf, A.F., Lowell, T. V, 2017. Hydrogen isotopes of *n*-
894 alkanes and *n*-alkanoic acids as tracers of precipitation in a temperate
895 forest and implications for paleorecords. Geochimica et Cosmochimica Acta
896 206, 166–183.
897 Froese, D.G., Zazula, G.D., Westgate, J.A., Preece, S.J., Sanborn, P.T., Reyes,
898 A. V., Pearce, N.J.G., 2009. The Klondike goldfields and Pleistocene
899 environments of Beringia. GSA Today 19, 4–10.
900 Gamarra, B., Sachse, D., Kahmen, A., 2012. Effects of leaf water evaporative

^{2}H-enrichment and biosynthetic fractionation on leaf wax *n*-alkane δ^{2}H values in C3 and C4 grasses. Plant, Cell and Environment 39, 2390-2403.

Gamarra, B., Kahmen, A., 2017. Low secondary leaf wax *n*-alkane synthesis on fully mature leaves of C3 grasses grown at controlled environmental conditions and variable humidity. Rapid Communications in Mass Spectrometry 31, 218–226.

Gao, L., Edwards, E.J., Zeng, Y., Huang, Y., 2014. Major Evolutionary Trends in Hydrogen Isotope Fractionation of Vascular Plant Leaf Waxes. PLoS ONE 9. doi:10.1371/journal.pone.0112610

Hou, J., D'Andrea, W.J., Huang, Y., 2008. Can sedimentary leaf waxes record D / H ratios of continental precipitation? Field, model, and experimental assessments. Geochimica et Cosmochimica Acta 72, 3503–3517.

Hou, J., D'Andrea, W.J., MacDonald, D., Huang, Y., 2007. Hydrogen isotopic variability in leaf waxes among terrestrial and aquatic plants around Blood Pond, Massachusetts (USA). Organic Geochemistry 38, 977–984.

Huang, Y., Eglinton, G., Ineson, P., Latter, P.M., Bol, R., Harkness, D.D., 1997. Absence of carbon isotope fractionation of individualnal *n*-alkanes in a 23-year field decomposition experiment with Calluna vulgaris. Organic Geochemistry 26, 497–501.

Jia, G., Wei, K., Chen, F., Peng, P., 2008. Soil *n*-alkane δD vs. altitude gradients along Mount Gongga, China. Geochimica et Cosmochimica Acta

72, 5165–5174.

Kahmen, A., Hoffmann, B., Schefuß, E., Arndt, S.K., Cernusak, L.A., West, J.B., Sachse, D., 2013. Leaf water deuterium enrichment shapes leaf wax *n* -alkane δD values of angiosperm plants II : Observational evidence and global implicatio ns. Geochimica et Cosmochimica Acta 111, 50–63.

Kahmen, A., Simonin, K., Tu, K.P., Merchant, A., Callister, A., Siegwolf, R., Dawson, T.E., Arndt, S.K., 2008. Effects of environmental parameters , leaf physiological properties and leaf water relations on leaf water $\delta^{18}O$ enrichment in different Eucalyptus species. Plant, Cell and Environment 31, 738–751.

Kaufman, D.S., Axford, Y., Schindler, D.E., Walker, I.R., Werner, A., 2012. A multi-proxy record of the Last Glacial Maximum and last 14,500 years of paleoenvironmental change at Lone Spruce Pond, southwestern Alaska. Journal of Paleolimnology 48, 9–26.

Kriticos, D.J., Webber, B.L., Leriche, A., Ota, N., Macadam, I., Bathols, J., Scott, J.K., 2012. CliMond: Global high-resolution historical and future scenario climate surfaces for bioclimatic modelling. Methods in Ecology and Evolution 3, 53–64.

Lee, H., Feakins, S.J., Lu, Z., Schimmelmann, A., Sessions, A.L., Tierney, J.E., Williams, T.J., 2017. Comparison of three methods for the methylation of aliphatic and aromatic compounds. Rapid Communications in Mass

943 Spectrometry 31, 1633–1640.

944 Lehmann, J., Solomon, D., Kinyangi, J., Dathe, L., Wirick, S.U.E., Jacobsen, C.,
945 2008. Spatial complexity of soil organic matter forms at nanometre scales.
946 Nature Geoscience 1, 238–242.

947 Liu, J., Liu, W., An, Z., Yang, H., 2016. Different hydrogen isotope
948 fractionations during lipid formation in higher plants: Implications for
949 paleohydrology reconstruction at a global scale. Scientific Reports 6, 1–10.

950 Mackay, J.R., 1983. Downward water movement into frozen ground, western
951 arctic coast, Canada. Canadian Journal of Earth Sciences 20, 120-134.

952 Matheus, P., Begét, J., Mason, O., Gelvin-Reymiller, C., 2003. Late Pliocene to
953 late Pleistocene environments preserved at the Palisades Site, central
954 Yukon River, Alaska. Quaternary Research 60, 33–43.

955 Matthews, J.V., Westgate, J.A., Ovenden, L., Carter, L.D., Fouch, T., 2003.
956 Stratigraphy, fossils, and age of sediments at the upper pit of the Lost
957 Chicken gold mine: new information on the late Pliocene environment of
958 east central Alaska. Quaternary Research 60, 9-18.

959 Nguyen Tu, T.T., Egasse, C., Anquetil, C., Zanetti, F., Zeller, B., Huon, S.,
960 Derenne, S., 2017. Leaf lipid degradation in soils and surface sediments: A
961 litterbag experiment. Organic Geochemistry 104, 35–41.

962 Nichols, J., Booth, R.K., Jackson, S.T., Pendall, E.G., Huang, Y., 2010.

963 Differential hydrogen isotopic ratios of *Sphagnum* and vascular plant
964 biomarkers in ombrotrophic peatlands as a quantitative proxy for
965 precipitation—evaporation balance. Geochimica et Cosmochimica Acta 74,
966 1407–1416.

967 Nichols, J.E., Peteet, D.M., Moy, C.M., Castañeda, I.S., Mcgeachy, A., Perez,
968 M., 2014. Impacts of climate and vegetation change on carbon
969 accumulation in a south-central Alaskan peatland assessed with novel
970 organic geochemical techniques. The Holocene 24, 1146–1155.

971 Pagani, M., Pedentchouk, N., Huber, M., Sluijs, A., Schouten, S., Brinkhuis, H.,
972 Dickens, G.R., Scientists, E., 2006. Arctic hydrology during global warming
973 at the Palaeocene/Eocene thermal maximum. Nature 442, 671–675.

974 Pancost, R.D., Baas, M., van Geel, B., Sinninghe Damsté, J.S., 2002.
975 Biomarkers as proxies for plant inputs to peats: an example from a sub-
976 boreal ombrotrophic bog. Organic Geochemistry 33, 675-690.

977 Pautler, B.G., Reichart, G.J., Sanborn, P.T., Simpson, M.J., Weijers, J.W.H.,
978 2014. Comparison of soil derived tetraether membrane lipid distributions
979 and plant-wax δD compositions compositions for reconstruction of
980 Canadian Arctic temperatures. Palaeogeography, Palaeoclimatology,
981 Palaeoecology 404, 78–88.

982 Peterse, F., van der Meer, M.T.J., Schouten, S., Jia, G., Ossebaar, J., Blokker,
983 J., Sinninghe Damsté, J.S., 2009. Assessment of soil *n*-alkane δD and

branched tetraether membrane lipid distributions as tools for paleoelevation reconstruction. Biogeosciences Discussions 6, 2799–2807.

Péwé, T.L., Westgate, J.A., Preece, S.J., Brown, P.M., Leavitt, S.W., 2009. Late Pliocene Dawson cut forest bed and new tephrochronological findings in the Gold Hill Loess, east-central Alaska. Bulletin of the Geological Society of America 121, 294–320.

Ponton, C., West, A.J., Feakins, S.J., Galy, V., 2014. Leaf wax biomarkers in transit record river catchment composition. Geophysical Research Letters 41, 6420–6427.

Porter, T.J., Froese, D.G., Feakins, S.J., Bindeman, I.N., Mahony, M.E., Pautler, B.G., Reichart, G.J., Sanborn, P.T., Simpson, M.J., Weijers, J.W.H., 2016. Multiple water isotope proxy reconstruction of extremely low last glacial temperatures in Eastern Beringia (Western Arctic). Quaternary Science Reviews 137, 113–125.

Preece, S.J., Westgate, J.A., Froese, D.G., Pearce, N.J.G., Perkins, W.T., 2011. A catalogue of late Cenozoic tephra beds in the Klondike goldfields and adjacent areas, Yukon Territory. Canadian Journal of Earth Science 48, 1386-1418.

Rao, Z., Zhu, Z., Jia, G., Henderson, A.C.G., Xue, Q., Wang, S., 2009. Compound specific δD values of long chain *n*-alkanes derived from terrestrial higher plants are indicative of the δD of meteoric waters:

1005 Evidence from surface soils in eastern China. Organic Geochemistry 40,
1006 922–930.

1007 Roden, J.S., Lin, G., Ehleringer, J.R., 2000a. A mechanistic model for
1008 interpretation of hydrogen and oxygen isotope ratios in tree-ring cellulose.
1009 Geochimica et Cosmochimica Acta 64, 21–35.

1010 Roden, J.S., Ehleringer, J.R., 2000b. There is no temperature dependence of
1011 net biochemical fractionation of hydrogen and oxygen isotopes in tree-ring
1012 cellulose. Isotopes in Enviromental and Health Studies 36, 303-317.

1013 Sachse, D., Billault, I., Bowen, G.J., Chikaraishi, Y., Dawson, T.E., Feakins,
1014 S.J., Freeman, K.H., Magill, C.R., McInerney, F. a., van der Meer,
1015 M.T.J.J., Polissar, P., Robins, R.J., Sachs, J.P., Schmidt, H.-L., Sessions,
1016 A.L., White, J.W.C., West, J.B., Kahmen, A., 2012. Molecular
1017 paleohydrology: interpreting the hydrogen-isotopic composition of lipid
1018 biomarkers from photosynthesizing organisms. Annual Review of Earth
1019 and Planetary Sciences 40, 221–249.

1020 Sachse, D., Dawson, T.E., Kahmen, A., 2015. Seasonal variation of leaf wax *n* -
1021 alkane production and δ^2H values from the evergreen oak tree, *Quercus*
1022 *agrifolia*. Isotopes in Environmental and Health Studies 51, 124–142.

1023 Sachse, D., Radke, J., Gleixner, G., 2004. Hydrogen isotope ratios of recent
1024 lacustrine sedimentary *n*-alkanes record modern climate variability.
1025 Geochimica et Cosmochimica Acta 68, 4877–4889.

1026 Sachse, D., Radke, J., Gleixner, G., 2006. δD values of individual *n* -alkanes
1027 from terrestrial plants along a climatic gradient – Implications for the
1028 sedimentary biomarker record. Organic Geochemistry 37, 469–483.

1029 Schäfer, I.K., Lanny, V., Franke, J., Eglinton, T.I., Zech, M., Vysloužilová, B.,
1030 Zech, R., 2016. Leaf waxes in litter and topsoils along a European transect.
1031 Soil 2, 551–564.

1032 Schwab, V.F., Garcin, Y., Sachse, D., Todou, G., Séné, O., Onana, J.M.,
1033 Achoundong, G., Gleixner, G., 2015. Effect of aridity on $\delta^{13}C$ and δD values
1034 of C3 plant- and C4 graminoid-derived leaf wax lipids from soils along an
1035 environmental gradient in Cameroon (Western Central Africa). Organic
1036 Geochemistry 78, 99–109.

1037 Schweger, C., Froese, D., White, J.M., Westgate, J.A., 2011. Pre-glacial and
1038 interglacial pollen records over the last 3 Ma from northwest Canada: Why
1039 do Holocene forests differ from those of previous interglaciations?
1040 Quaternary Science Reviews 30, 2124–2133.

1041 Sessions, A.L., 2006. Seasonal changes in D/H fractionation accompanying lipid
1042 biosynthesis in Spartina alterniflora. Geochimica et Cosmochimica Acta
1043 70, 2153–2162.

1044 Sessions, A.L., Sylva, S.P., Summons, R.E., Hayes, J.M., 2004. Isotopic
1045 exchange of carbon-bound hydrogen over geologic timescales. Geochimica
1046 et Cosmochimica Acta 68, 1545–1559.

1047 Shanahan, T.M., Hughen, K.A., Ampel, L., Sauer, P.E., Fornace, K., 2013.
1048 Environmental controls on the $^{2}H/^{1}H$ values of terrestrial leaf waxes in the
1049 eastern Canadian Arctic. Geochimica et Cosmochimica Acta 119, 286–301.
1050 Smith, F.A., Freeman, K.H., 2006. Influence of physiology and climate on δD of
1051 leaf wax *n*-alkanes from C3 and C4 grasses. Geochimica et Cosmochimica
1052 Acta 70, 1172–1187.
1053 Soja, A.J., Tchebakova, N.M., French, N.H.F., Flannigan, M.D., Shugart, H.H.,
1054 Stocks, B.J., Sukhinin, A.I., Parfenova, E.I., Chapin, F.S., Stackhouse,
1055 P.W., 2007. Climate-induced boreal forest change: Predictions versus
1056 current observations. Global and Planetary Change 56, 274–296.
1057 Tierney, J.E., Russell, J.M., Huang, Y., Damste, J.S.S., Hopmans, E.C., Cohen,
1058 A.S., 2008. Northern Hemisphere Controls on Tropical Southeast African
1059 Climate During the Past 60,000 Years. Science 322, 252–255.
1060 Tipple, B.J., Berke, M.A., Doman, C.E., Khachaturyan, S., Ehleringer, J.R.,
1061 2013. Leaf-wax *n*-alkanes record the plant-water environment at leaf flush.
1062 Proceedings of the National Academy of Sciences 110, 2659–2664.
1063 Turetsky, M.R., Bond-Lamberty, B., Euskirchen, E., Talbot, J., Frolking, S.,
1064 McGuire, A.D., Tuittila, E-S., 2012. The resilience and functional role of
1065 moss in boreal and arctic ecosystems. New Phytologist 196, 49-67.
1066 USNO-AA (U.S. Naval Observatory, Astronomical Applications Department),
1067 2018. Available at: http://aa.usno.navy.mil/data/docs/Dur_OneYear.php.

1068 Viau, A.E., Gajewski, K., Sawada, M.C., Bunbury, J., 2008. Low- and high-
1069 frequency climate variability in eastern Beringia during the past 25,000
1070 years. Canadian Journal of Earth Sciences 45, 1435-1453.

1071 Vonk, J.E., Tesi, T., Bröder, L., Holmstrand, H., Hugelius, G., Andersson, A.,
1072 Dudarev, O., Semiletov, I., Gustafsson, Ö., 2017. Distinguishing between
1073 old and modern permafrost sources in the northeast Siberian land-shelf
1074 system with compound-specific δ^2H analysis. Cryosphere 11, 1879–1895.

1075 Wahl, H., 2004. Ecoregions of the Yukon Territory: Biophysical Properties of
1076 Yukon Landscapes, in: Smith, C.A.S., Meikle, J.C., Roots, C.F. (Eds.),
1077 PARC Technical Bulletin No. 04-01. Agriculture and Agri-Food Canada,
1078 Summerland, British Columbia, p. 313.

1079 White, J.W.C., Cook, E.R., Lawrence, J.R., Wallace S., B., 1985. The ratios of
1080 sap in trees: Implications for water sources and tree ring ratios.
1081 Geochimica et Cosmochimica Acta 49, 237–246.

1082 Wilkie, K.M.K., Chapligin, B., Meyer, H., Burns, S., Petsch, S., Brigham-
1083 Grette, J., 2013. Modern isotope hydrology and controls on δD of plant leaf
1084 waxes at Lake El'gygytgyn, NE Russia. Climate of the Past 9, 335–352.

1085 Yang, H., Huang, Y., 2003. Preservation of lipid hydrogen isotope ratios in
1086 Miocene lacustrine sediments and plant fossils at Clarkia, northern Idaho,
1087 USA. Organic Geochemistry 34, 413–423.

1088 Yang, H., Pagani, M., Briggs, D.E.G., Equiza, M.A., Jagels, R., Leng, Q.,

Lepage, B.A., 2009. Carbon and hydrogen isotope fractionation under continuous light: implications for paleoenvironmental interpretations of the High Arctic during Paleogene warming. Oecologia 160, 461–470.

Zazula, G.D., Froese, D.G., Schweger, C.E., Mathewes, R.W., Beaudoin, A.B., Telka, A.M., Harington, C.R., Westgate, J.A., 2003. Ice-age steppe vegetation in East Beringia. Nature 423, 603.

Zazula, G.D., Froese, D.G., Elias, S.A., Kuzmina, S., Mathewes, R.W., 2011. Early Wisconsinan (MIS 4) Arctic ground squirrel middens and a squirrel-eye-view of the mammoth-steppe. Quaternary Science Reviews 30, 2220-2237.

Zhou, Y., Grice, K., Stuart-Williams, H., Farquhar, G.D., Hocart, C.H., Lu, H., Liu, W., 2010. Biosynthetic origin of the saw-toothed profile in $\delta^{13}C$ and $\delta^{2}H$ of *n*-alkanes and systematic isotopic differences between *n*-, *iso*- and *anteiso*-alkanes in leaf waxes of land plants. Phytochemistry 71, 388–403.

Figure Captions

Fig. 1. Regional maps of (a) annual precipitation (mm/year) (WorldClim 2) and (b) mean annual temperature (°C) (WorldClim 2), with locations of the study sites (black dots), local GNIP sites (white triangles), and the Arctic circle (thin black line), north of which sites experience 24-hr daylight at least one day per year. For colour version of figure, refer to the online version of the article.

Fig. 2. Average monthly δD_{precip} (OIPC), mean air temperature (ERA-Int), and precipitation (WorldClim 2). Error bars represent the range of values for each of the study sites.

Fig. 3. *n*-Acid relative abundance distributions for (a-e) type-averaged vegetation and (f) soils. The total number (n) of samples analysed is indicated. The *n*-acid distributions reflect regional averages for each vegetation type and soil, first averaged by site and then the site averages were used to calculate regional averages. Error bars represent 1σ.

Fig. 4. Site-averaged $\varepsilon_{wax/MAP}$ for *n*-C_{24}, -C_{26}, and -C_{28} acids (red, grey and blue circles, respectively) versus: (a) latitude, (b) elevation (m a.s.l.), (c) annual precipitation (mm; WorldClim 2), (d) mean annual air temperature (°C; ERA-

Interim), (e) mean growing season air temperature (May-September), and (f) Summer (JJA) relative humidity (%; CliMond). Correlations significant at $p \leq 0.05$ are indicated. Box plots (g) of site-averaged $\varepsilon_{wax/MAP}$ values for *n*-C_{24} (red), -C_{26} (grey), and -C_{28} (blue) acids grouped by latitude (< 65°N and > 65°N); the n-C_{26} and -C_{28} group means are significantly different ($p \leq 0.05$; 2-sample t-test). For colour version of figure, refer to the online version of the article.

Fig. 5. (a) Comparison of sediment-derived $\varepsilon_{wax/MAP}$ values from other studies > 60°N, including *n*-acids and -alkanes; (b) map of corresponding site locations. The numeric codes refer to: [1] this study; [2] Wilkie et al. (2013); [3] Daniels et al. (2017); (4) Shanahan et al. (2013); [5] Sachse et al. (2006). For colour version of figure, refer to the online version of the article.

Fig. 6. OIPC-δD_{MAP} for the study sites versus (a) latitude and (c) mean annual temperature. δD_{wax} (*n*-$C_{24,26,28}$ acids; red, grey and blue circles, respectively) for the study sites versus (b) latitude and (d) mean annual temperature. For colour version of figure, refer to the online version of the article.

Table Captions

Table 1: Sampling site locations and mean climate

Table 2: Site-averaged δD_{wax} and $\delta_{wax/MAP}$ for n-$C_{24\text{-}28}$ acids in topsoil (0-30 cm) samples

Table 1

Site		Location			Temperature (°C)[a]		Precipitation (mm)[b]		Relative Humidity (%)[c]	
Code	Full Name	Lat.	Long.	Elev. (m a.s.l)	MAT	MJJAS	Annual	MJJAS	Annual	JJA
SP	Spindly Pine Lake	60.302	–134.992	792	–2.6	6.9	387	162	70.2	65.4
WH	Whitehorse	60.812	–135.211	729	–1.7	8.1	250	151	68.4	62.9
TKR	Takhini River	60.852	–135.718	662	–2.0	7.8	254	148	69.3	64.3
KL	Kluane Lake	60.965	–138.059	950	–4.5	4.2	363	204	74.6	74.1
MYO	Mayo	63.541	–136.162	555	–3.5	9.4	325	205	68.3	61.5
BRM	Brimstone	63.742	–138.849	639	–2.9	10.1	329	206	70.9	68.1
LC	Lost Chicken	64.068	–141.911	588	–4.9	9.2	249	192	70.9	68.3
SH	Scree Hill	65.071	–138.155	875	–6.7	6.7	376	224	69.0	65.8
DHP174	Dempster Hwy Peatland	65.212	–138.327	738	–6.4	7.0	359	229	69.0	65.6
EAG	Eagle Plains	66.444	–136.675	370	–6.7	8.3	333	186	67.9	63.6
TSI	Tsiigehtchic	68.042	–133.489	78	–7.0	9.0	241	140	67.5	62.5
CL	Campbell Lake	68.207	–133.406	46	–8.4	8.0	242	140	67.5	62.5
INU	Inuvik	68.315	–133.553	58	–8.4	8.0	238	137	67.5	62.5

[a]ERA-Interim surface temperature data (1981-2010), (~80 km spatial resolution) mean annual temperature and mean temperature May-September (Dee et al., 2011)

[b]WorldClim2 precipitation data, annual (30" spatial resolution) and total May-September (Fick and Hijmans, 2017)

[c]CliMond humidity data (10' spatial resolution), annual and average May-September (Kriticos et al., 2012)

Table 2

		δD_{wax} (‰) ± 1σ (*n*)			$\varepsilon_{wax/MAP}$ (‰) ± 1σ (*n*)		
Site	δD_{MAP} (‰)[a]	C_{24}	C_{26}	C_{28}	C_{24}	C_{26}	C_{28}
SP	–163	–237 ± 6.9 (9)	–258 ± 7.5 (9)	–255 ± 11.7 (9)	–88 ± 8.3 (9)	–114 ± 9.0 (9)	–110 ± 14.0 (9)
WH	–165	–252 (1)	–250 ± 2.6 (3)	–244 ± 5.0 (3)	–104 (1)	–101 ± 3.1 (3)	–95 ± 6.0 (3)
TKR	–164	–240 ± 3.9 (5)	–249 ± 9.9 (5)	–247 ± 6.3 (3)	–91 ± 4.7 (5)	–102 ± 11.8 (5)	–100 ± 7.5 (3)
KL	–167	–243 (1)	–254 (1)	–242 (1)	–92 (1)	–105 (1)	–91 (1)
MYO	–161	–253 ± 1.8 (2)	–264 ± 2. (2)	–255 ± 2.4 (2)	–110 ± 2.1 (2)	–122 ± 2.4 (2)	–111 ± 2.8 (2)
BRM	–164	–245 ± 2.9 (3)	–246 ± 5.9 (3)	–248 ± 3.9 (3)	–97 ± 3.4 (3)	–98 ± 7.0 (3)	–101 ± 4.7 (3)
LC	–160	–242 ± 7.8 (2)	–251 ± (1)	–243 (1)	–98 ± 9.3 (2)	–109 (1)	–99 (1)
SH	–174	–253 ± 12.6 (3)	–261 ± 5.9 (2)	–260 ± 5.7 (2)	–95 ± 15.2 (3)	–105 ± 7.1 (2)	–104 ± 6.9 (2)
DHP174	–173	–243 ± 7.6 (3)	–255 ± 4.2 (3)	–239 ± 2.3 (3)	–84 ± 9.2 (3)	–99 ± 5.1 (3)	–80 ± 2.8 (3)
EAG	–171	–256 ± 2.7 (4)	–255 ± 8.1 (4)	–252 ± 8.4 (3)	–102 ± 3.2 (4)	–102 ± 9.8 (4)	–98 ± 10.1 (3)
TSI	–175	–244 ± 2.5 (3)	–241 ± 8.7 (2)	–238 ± 4.3 (2)	–84 ± 3.1 (3)	–80 ± 10.6 (2)	–77 ± 5.2 (2)
CL	–176	–253 ± 2.2 (2)	–256 ± 6.7 (2)	–248 ± 8.2 (2)	–94 ± 2.6 (2)	–97 ± 8.1 (2)	–87 ± 9.9 (2)
INU	–176	–234 ± 5.0 (2)	–244 ± 6.7 (2)	–247 (1)	–71 ± 6. (2)	–82 ± 8.1 (2)	–87 (1)
Mean	–168	–246	–253	–248	–93	–101	–95
1σ	6.0	6.8	6.6	6.4	10.0	11.3	10.7

[a]OIPC δD_{MAP} (Bowen and Revenaugh, 2003)

Figure 1

Click here to download high resolution image

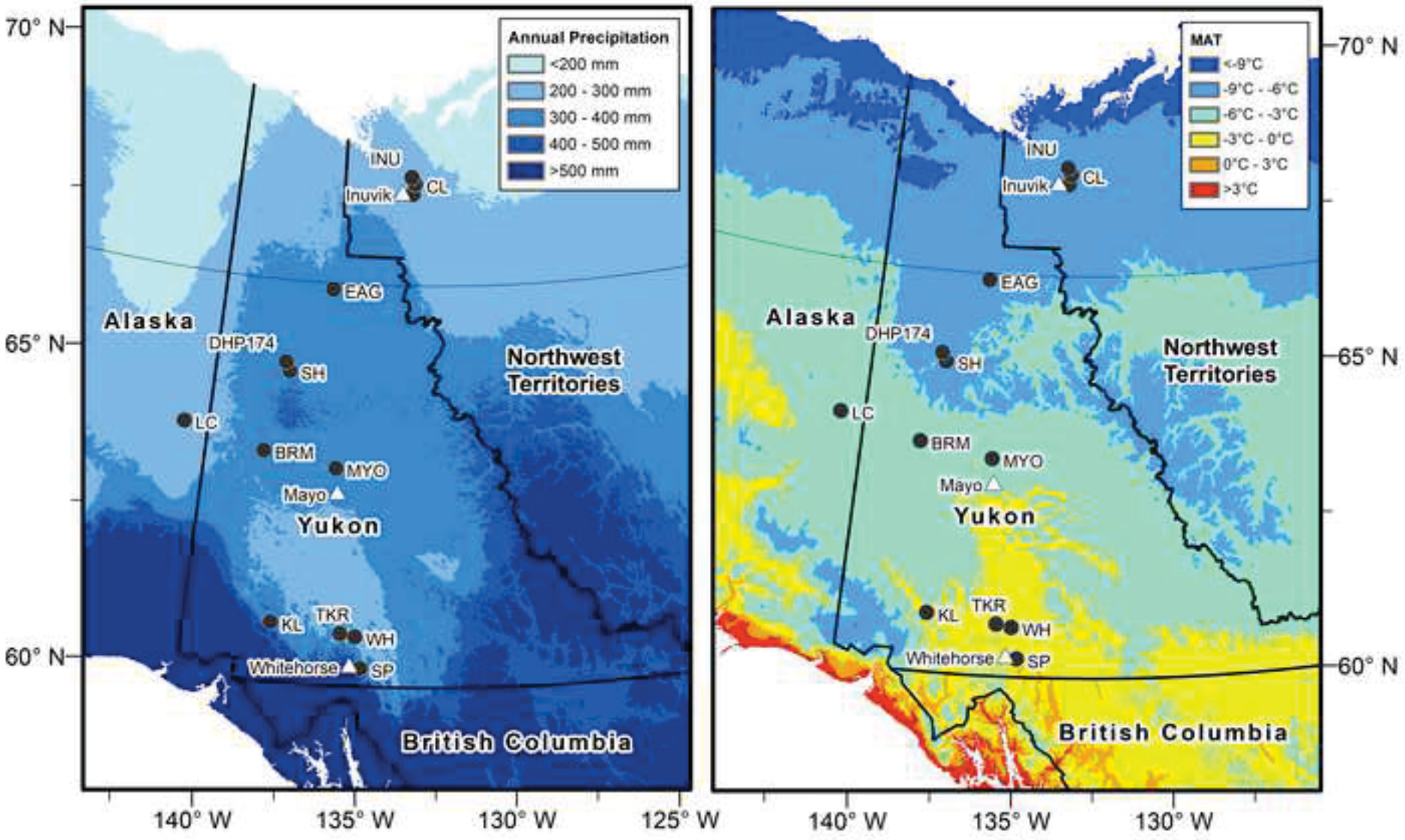

Figure 2

Click here to download high resolution image

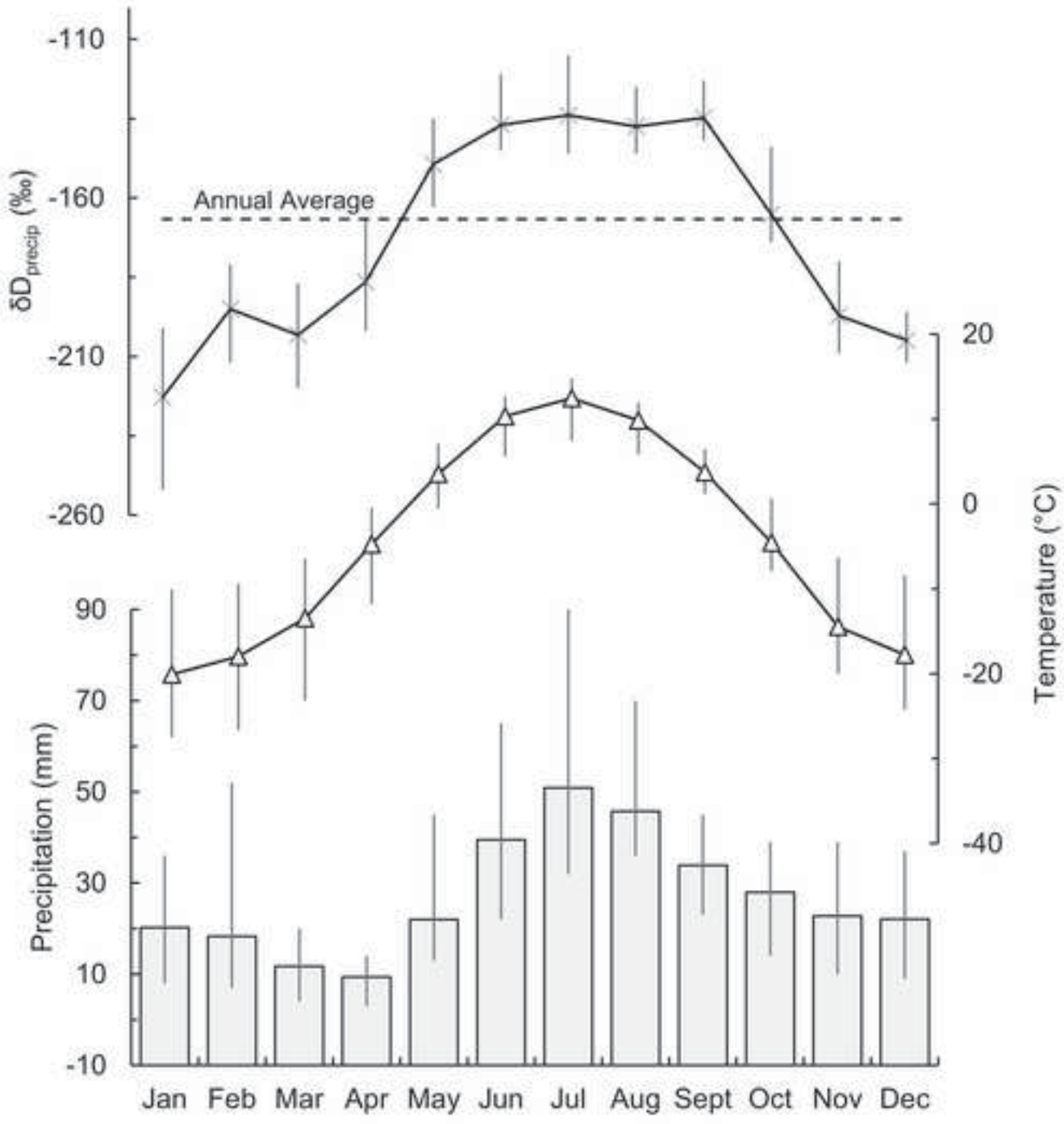

Figure 3

Click here to download high resolution image

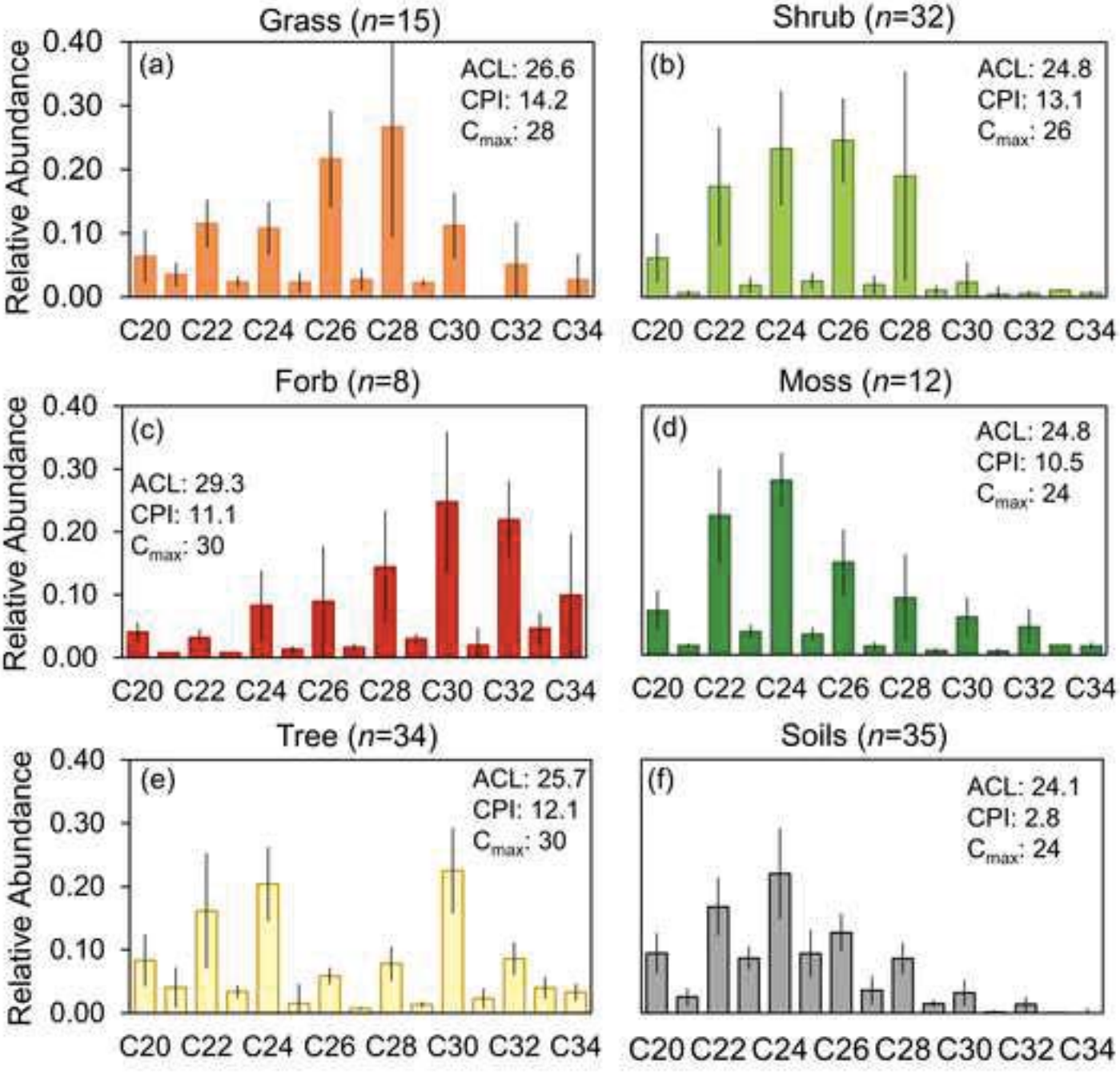

Figure 4

Click here to download high resolution image

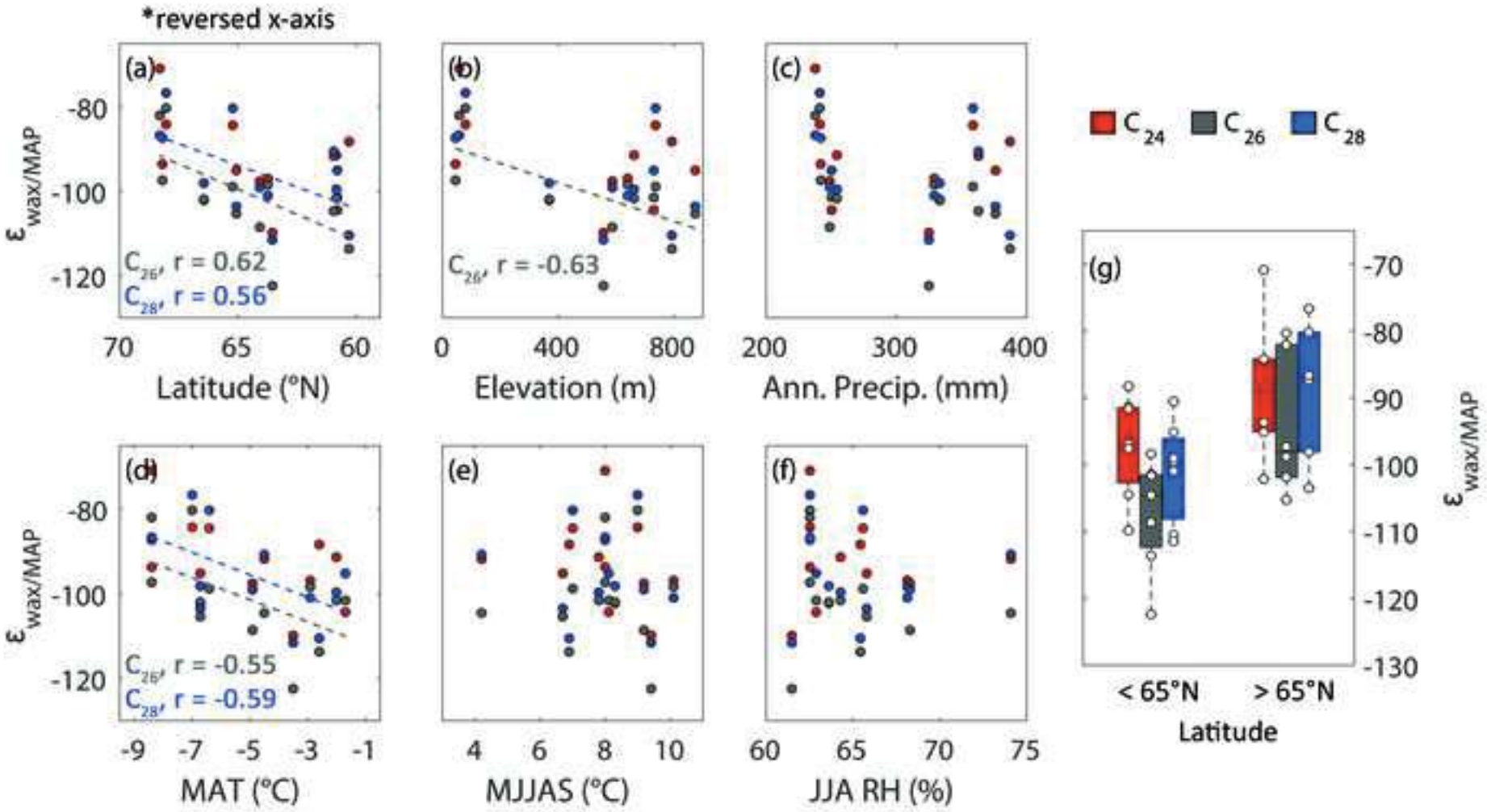

Figure 5

Click here to download high resolution image

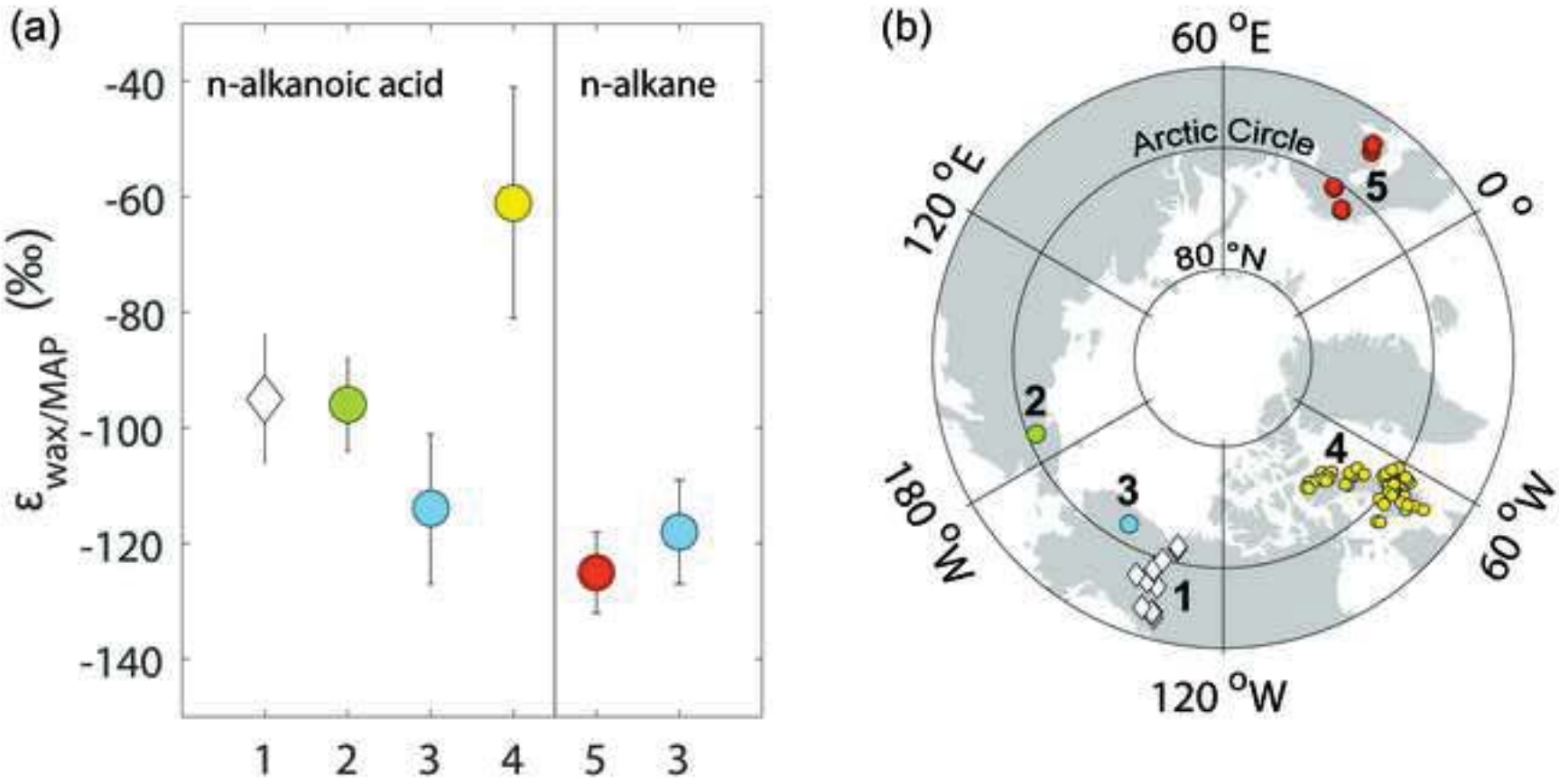

Figure 6

Click here to download high resolution image